

FACULTY OF SCIENCE AND ENGINEERING
LINKÖPING UNIVERSITY

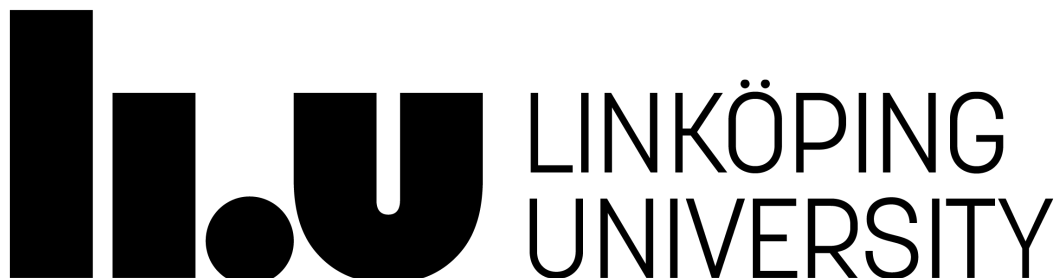
Thesis submitted for the bachelor's degree in
Aerospace Engineering

LIU-IEI-TEK-A-23/04735—SE

Exploration Of Force Control in UAV Actuators

by

Adam El Ghaib



Supervisor: **David Lundström**

June 2023

Declaration of Original and Sole Authorship

I, Adam El Ghaib, declare that this thesis entitled *Exploration Of Force Control in UAV Actuators* and the data presented in it are original and my own work.

I confirm that:

- No part of this work has previously been submitted for a degree at this or any other university.
- References to the work of others have been clearly acknowledged. Quotations from the work of others have been clearly indicated, and attributed to them.
- In cases where others have contributed to part of this work, such contribution has been clearly acknowledged and distinguished from my own work.

Date: June 2023

Signature:

A handwritten signature in black ink, appearing to read "Adam El Ghaib". It is written in a cursive style with a horizontal line extending from the end of the signature.

Abstract

Exploration Of Force Control in UAV Actuators

Unmanned air vehicles (UAV) rely on fly-by-wire (FBW) to control the actuators and therefore to control the vehicle. Common actuators only allow changing the position of the control surface thus, "stick-free" flight can not be reproduced in UAV. In this project, ways of maintaining a certain amount of force produced by a canard wing constant in front of, external perturbations in the wind speed, and angle of attack over time are explored. That is to say, reproducing a "stick-free" flight in UAV. This would allow flying unstable UAV configurations and having an additional flight control system (FCS) that could be used for redundancy. Previous work to control the force delivered by an actuator has been applied in robotics for surface polishing or in cinematography for camera stabilization. Nevertheless, in model airplanes, direct force control techniques are seldom used. The methodology followed in this project has been to study which force control strategies have been successfully done in the past. Afterwards, four proofs of concept have been proposed and two of them have been built and analyzed. The results have shown that both concepts attain the aim of the project, nonetheless, both have drawbacks and advantages and some design parameters such as volume, weight, or power can be improved.

Key words: UAV, Actuator, Force, Control, Conceptual, Design, Gimbal, Motor, Spring, Potentiometer, Magnetic, Sensor, FOC.

Acknowledgment

The delivery of this project represents a milestone in my education as an aerospace engineer, but also in my personal life. This would not have been possible without the support of my family, teachers and friends.

To my family, Aya, Yasmin, Driss and Aicha thanks for always believing in me and bringing me support when I needed it the most.

To my teachers, I am grateful for all the things you have taught me, not only academically but also personally. Especially, I would like to express my gratitude to my supervisor David Lündstrom, who has guided me through the development of this project and provided me with useful insights.

To my friends, thank you all for helping me become a better professional and a better person, my education would not have been the same without you. Special thanks to Salva for showing me that you can always be a better version of yourself, Steven for all the good times we shared at University and Jan for his valuable advice.

Abbreviations

AC	Alternating Current
BLDCM	Brush Less Direct Current Motor
CAD	Computer Aid Design
CFD	Computer Fluid Dynamics
DC	Direct Current
DLC	Direct Lift Control
EMA	Electro Mechanical Actuator
EMI	Electro Magnetic Interference
ESC	Electronic Speed Controller
eVTOL	electrical Vertical Take-off Landing
FBW	Fly-By-Wire
FCS	Flight Control System
FEM	Finite Element Method
FLUMES	Fluida och mekatroniska system
FOC	Field Oriented Control
HA	Hydraulic Actuator
LE	Leading Edge
LLT	Lifting Line Theory
MAC	Mean Aerodynamic Chord
MEA	More Electric Aircraft
MOSFET	Metal Oxide Semiconductor Field-Effect Transistors
OWA	Ordered Weighted Average
PI	Proportional Integral
PWM	Pulse Width Modulation
SPWM	Sinusoidal Pulse Width Modulation
TE	Trailing Edge
UAV	Unmanned Air Vehicle
VFD	Variable Frequency Driver

Nomenclature

α	Angle of attack [°]	l	Distance [m]
β	Slip angle [°]	m	Mass [kg]
γ	Pitch angle [°]	q	Dynamic pressure [Pa]
ϵ	Strain	s	Lever arm distance [m]
ζ	Controller damping ratio [°]	v	Velocity [m/s]
θ	Angular position [°]	x_{ac}	Distance to aerodynamic center [m]
κ	Gauge intrinsic factor	x_{cg}	Distance to gravity center [m]
ν	Kinematic viscosity [m^2/s]	x_h	Distance to hinge [m]
π	Number Pi	AR	Aspect ratio
ρ	Density [Kg/m^3]	B	Mechanical damping ratio [Kg/s]
σ	Stress [Pa]	C_D	Drag coefficient
τ	Torque [$N \cdot m, Kg \cdot cm$]	C_{D0}	Parasite drag coefficient
ϕ	Magnetic encoder angle [°]	C_{Di}	Induced drag coefficient
ω	Angular speed [°/s]	C_{he}	Hinge moment coefficient
Γ	Flow circulation	C_{h0}	Zero hinge moment coefficient
Λ	Sweep angle [°/s]	C_{ha}	Alpha hinge moment coefficient
a	Acceleration [m/s^2]	C_f	Skin friction coefficient
b	Wingspan [m]	C_L	Lift coefficient
c_r	Root chord [m]	C_{L0}	Zero lift coefficient
c_t	Tip chord [m]	$C_{L\alpha}$	Alpha lift coefficient
e	Oswald efficiency number	D	Drag force [N]
f	Frequency [Hz]	F	Force [N]
g	Gravitational constant [m/s^2]	H	Hinge moment [$N \cdot m$]
c_r	Root chord [m]	I, J	Mass moment of inertia [$Kg \cdot m^2$]
c_t	Tip chord [m]	L	Lift force [N]
f	Frequency [Hz]	M	Mach number
g	Earth's surface gravitational constant [m/s^2]	M_{ac}	Free aerodynamic center moment [$N \cdot m$]
i_w	Wing initial incidence angle [°]	P	Static pressure [Pa]
k	Spring constant [N/m]	R	Electrical resistance [Ω]
k_d	Derivative gain	Re	Reynold's number
k_i	Integral gain	S	Surface [m^2]
k_p	Proportional gain	S_{ref}	Wing reference surface [m^2]
k_t	Torque constant	U_∞	Undisturbed wind speed [m/s]
		V	Voltage [V]

Contents

Declaration of Original and Sole Authorship	iii
Abstract	v
Acknowledgment	vii
Abbreviations	ix
Nomenclature	xi
Contents	xiii
List of Figures	xvii
List of Tables	xix
Introduction	1
1 Introduction	1
1.1 Aim	2
1.2 Scope	2
1.3 Delimitations	2
1.4 Deliverables	2
1.5 Requirements	3
1.6 Background	3
1.7 Methodology	3
1.8 Outline	3
2 Research & Aerodynamic Analysis	5
2.1 State of The Art	5
2.1.1 Flight Control Systems	6
2.1.2 Fly-By-Wire	7
2.1.3 UAV Flight Control	7
2.1.4 Flight Control Surfaces	8
2.1.5 Frames of reference	8
2.2 Control Surface Aerodynamic Analysis	11
2.2.1 Lift & Drag	11

2.2.2	Hinge moment	12
2.3	Actuators & Sensors	17
2.3.1	Potentiometer	17
2.3.2	Load Cell	18
2.3.3	Electromechanical Actuators	18
2.3.4	Fluid power actuators	20
2.4	Control	21
2.4.1	Electronic Speed Control	21
2.4.2	Encoders	24
3	Concept Generation, Evaluation & Development	25
3.1	System Development Process	25
3.2	Force Transducers	26
3.2.1	Concept 1	26
3.2.2	Concept 2	27
3.3	Pressure Control	28
3.4	Direct Motor Control	28
3.4.1	Concept 3	28
3.4.2	Concept 4	30
3.5	Concept Evaluation	30
3.5.1	Ordered Weighted Average	30
3.5.2	Additional Evaluations	31
3.6	Concept Development	32
3.6.1	Working principles	32
3.6.2	Equipment Definition & Sizing	36
3.6.3	Final Design & Code	42
4	Analysis & Results	49
4.1	Resonance Frequency	49
4.1.1	Mechanical resonance frequency	49
4.1.2	Electrical resonance frequency	51
4.2	Models performance	52
4.3	Improvements	54
4.4	Next steps	55
Conclusion		57
Bibliography		59
A Codes		63
A.1	Actuator sizing	63
A.2	Spring sizing	64
A.3	Concept 1 full code	65

A.4 Concept 4 full code	66
A.5 Concept 4 Position & Force Control	68
B Drawings	73

List of Figures

2.1	Flight control systems. Extracted from p.5-2 [19]	6
2.2	Basic elements of a fly-by-wire flight control system. Extracted from p.180 [18]	7
2.3	Flight control angles and moments in body frame. Extracted from p.4 [26]	8
2.4	3D representation of the Euler angles. Extracted from p.118 [18]	9
2.5	Airfoil lift coefficient vs alpha obtained applying experimentally. Extracted from [28]	11
2.6	Numerical wing lift coefficient vs alpha obtained applying LLT in XFLR5[8].	11
2.7	Graphic method to obtain the location of the MAC.	13
2.8	(a) Hinge moment coefficient vs alpha, (b) torque needed to maintain a specific angle of attack vs velocity, (c) for constant torque, alpha in front of velocity.	14
2.9	Torque produced at the hinge against the angle of attack.	16
2.10	Block diagram for mechatronic systems. Extracted from p.4 [23]	17
2.11	Potentiometer wiring diagram. Extracted from [15]	17
2.12	Full Wheatstone bridge. Extracted from [6]	18
2.13	BLDCM diagram. Extracted from [1]	19
2.14	Servo motor parts. Extracted from [7]	19
2.15	EMA for the MEA. Extracted from [21]	19
2.16	Geometry of hydraulic actuator. Extracted from p.134 [23]	20
2.17	The typical structure of the HA system. Extracted from [29]	21
2.18	ECS schematic. Extracted from [3]	22
2.19	Trapezoidal commutation. Extracted from[24]	22
2.20	Sinusoidal pulse width modulation. Extracted from [24]	23
2.21	Rotor's and stator's magnetic field. Extracted from [4]	23
2.22	Incremental encoder signal combinations. Extracted from [5]	24
3.1	FCS design process as defined by the V-model. Extracted from p.45 [26] . .	25
3.2	Concept 1, simplified scheme.	26
3.3	Concept 2, simplified scheme.	27
3.4	DC motor block diagram.	28
3.5	Reduced DC motor block diagram.	28
3.6	Simplified DC motor block diagram.	29
3.7	Closed loop control diagram of DC motor.	29
3.8	Concept 3, simplified scheme.	29
3.9	Concept 4, simplified scheme.	30

3.10	Concept 1, 2D geometric scheme.	32
3.11	Rotor and stator magnetic fields. Extracted from [24]	34
3.12	FOC implementation block diagram. Extracted from [16]	35
3.13	Servo motor MKS DS6630 [13].	36
3.14	Arduino UNO board [9].	36
3.15	Potentiometer P11S1V0FLSY00503KA [14].	37
3.16	Lever, CAD.	37
3.17	Rod, CAD.	38
3.18	Torque values at the hinge for each phi and theta angle.	39
3.19	Tension spring [17].	39
3.20	Stress over strain diagram for nylon 66. Extracted from p. 528 [22]	40
3.21	Gimbal motor iPower Motor GM5208-24 [11].	41
3.22	SimpleFOC board [10].	41
3.23	AS5X47U-TS-EK-AB magnetic encoder [12].	42
3.24	Concept 1, CAD.	42
3.25	Concept 4, wiring diagram	44
3.26	Concept 4, CAD.	45
3.27	Concept 4, wiring diagram Extracted from [2]	47
4.1	Concept 1, real model.	53
4.2	Concept 4, real model.	53
4.3	Size comparison between springs.	55

List of Tables

1.1 Requirements of the project.	3
2.1 Canard wing geometric parameters.	11
2.2 Advantages and drawbacks of Hydraulic and Pneumatic actuators.	20
3.1 Materials for concept 1.	26
3.2 Concept 1, advantages and drawbacks.	27
3.3 Materials for concept 2.	27
3.4 Concept 2, advantages and drawbacks.	27
3.5 Concept 3, advantages and drawbacks.	29
3.6 Materials for concept 3.	29
3.7 Concept 4, advantages and drawbacks.	30
3.8 Materials for concept 4.	30
3.9 OWA of design concepts.	31
3.10 MKS DS6630 specifications.	36
3.11 Potentiometer specifications.	37
3.12 Values of torque local maximum and minimum.	39
3.13 Tension spring specifications.	39
3.14 iPower Motor GM5208-24 specifications.	41
3.15 AS5X47U-TS-EK-AB specifications.	42

Chapter 1

Introduction

Unmanned air vehicles (UAVs) have been proven to be a practical tool in society, for both military applications such as reconnaissance and surveillance missions or civil demands such as cartography, crop spraying or inspecting public facilities. However, their complete range of capabilities is still unknown, new approaches to the use of this technology could astound the markets and help civilization to move forward technologically.

Reliability and safety in these kinds of systems are always a must. Before launching a new flight vehicle design to the market, it has to be certified by the pertinent authorities and several tests have to be carried out. The use of sub-scale unmanned aircraft for testing is particularly attractive as it is more economical and no pilot is required. Nevertheless, with conventional position actuators, the flight mechanics of a manned aircraft with mechanical control systems such as pulleys, push-rods, and wires, can not be fully reproduced. In order to do so, a way of directly setting the force produced by the control surfaces has to be implemented. In this manner, the force produced by the pilot can be imitated and force control is achieved. In addition, by achieving force control, unstable aircraft configurations may be able to be flown as the force produced by the control surface remains constant over the angle of attack or wind speed velocity perturbations.

In this thesis, methods to set the control surfaces based on delivering force instead of changing directly the position are studied and proposed as a control system for a fixed-wing canard configuration UAV fighter model.

1.1 Aim

The main objective of this project is to design a prototype system(s) capable of delivering and controlling directly the torque given to a canard wing.

1.2 Scope

To attain this objective the following topics are covered.

- Research about available force control techniques.
- Aerodynamic study of the control surface geometry.
- Concept generation of means to achieve force control.
- Concept evaluation and selection.
- Design and construction of horizontal stabilizer model(s) for testing purposes.

1.3 Delimitations

Next subjects are not included in the scope of this project.

- Study of lateral and vertical stability.
- Design of actuators.
- Assembly of the horizontal stabilizer model in the final aircraft configuration.
- Computational fluid dynamics (CFD) or finite element method (FEM) analysis of the model(s).

1.4 Deliverables

1. Assessment matrix of the proposed force control concepts.
2. Schematic of all the electronics used and the connections made for the selected concept.
3. Drawings of CAD model.
4. Constructed horizontal stabilizer model.
5. Full report delivery.

1.5 Requirements

CODE	REQUIREMENT	SOURCE
REQ-1	The control surface shall operate at 150 km/h	Customer
REQ-2	Angle of attack range shall be between $\pm 20^\circ$	Customer
REQ-3	Force control system shall be lightweight	Customer
REQ-4	The system shall operate between $6\text{-}8 \text{ V}$	Customer

Table 1.1: Requirements of the project.

1.6 Background

The main reason this project is carried out, is because of the need of the *Fluida och mekatroniska system* (FLUMES) department, at Linköping University of implementing an alternative longitudinal stability flight control system (FCS) in a fixed-wing fighter UAV with canard configuration. Which, can be able of mimicking the flight mechanics of a manned aircraft with a mechanical control system.

At the FLUMES department, several down-scaled prototypes of real aircraft are manufactured for scientific purposes. This allows to perform tests to validate and verify control strategies and aircraft systems before implementing them in the real models. Even though conventional position control does not usually fail, a mismatched or decalibrated controller could cause critical situations as fighter aircraft are naturally unstable and constantly rely on their control surfaces to fly. For these reasons, having backup control systems becomes such an important issue. In addition, the possibility to change from position control to force control allows the aircraft to be more versatile.

Secondly, this project will allow the author to go deeper into the different disciplines taught in the degree to solve a problem of the real aeronautical sector.

1.7 Methodology

To reach the objectives, the methodology followed consists in reviewing which force control techniques have been successfully developed in the past. A shallow study of different actuators and sensors that could potentially be used in the preliminary design is carried out.

Afterwards, taking into account the research done, four conceptual designs are proposed. With an assessment matrix that evaluates different criteria, the preliminary designs are compared, and two are selected for further development.

Finally, the selected prototypes are built and tested experimentally and their performance is evaluated.

1.8 Outline

In Chapter 1 a theoretical review about the state of the art of flight control systems, flight mechanics, actuators, sensors and control theory is carried out, furthermore, an

aerodynamic analysis of the control surface and a preliminary equipment sizing is done. In Chapter 2 different conceptual designs to achieve force control are proposed and after a detailed evaluation, some of the concepts are selected for further development. Finally, Chapter 3 presents the results of the experimental models and future improvements are proposed.

Chapter 2

Research & Aerodynamic Analysis

This chapter will start introducing the state of the art of FCS, focusing on fly-by-wire (FBW) strategies. Next, basic concepts about flight mechanics are studied. Then, aerodynamic analysis of the control surface and preliminary equipment sizing is done. Finally, this chapter ends by investigating different types of actuators that could be suitable options to reach force control, and some fundamentals of control strategies are reviewed.

2.1 State of The Art

Force control is understood as the action of controlling the force produced by any device, it could be from a force delivered by an actuator to a load, to the lift force produced by a wing. This concept is nothing new, and it has been used widely in robotic applications.

In robotics, force control is a technology developed to improve automated manufacturing processes. Parts produced in automatic chains, usually meet the dimensional specifications but still require additional processing to achieve desired surface finish. According to Edwin A. Erlbacher, nowadays, there are two commercially accepted methods of force control used in automated surface finishing [20]. "Through-the-arm" force control consists of closed-loop control. It is accomplished by mounting a torque/force transducer to the robot's wrist. The output signal of the transducer is fed back to the robot controller and the error is determined. Complications arise with this method because the force transducer and arm robot position act together becoming a coupled system. "Around-the-arm" de-couples the force control from the robot servo motors by using an independent device to control the force of the tool attached to the robot wrist.

In aeronautics, force control is mainly used as a method to compensate for the adverse effect of external disturbances and as a backup system to conventional position control. K. Yokota and H. Fujimoto [32] developed an aerodynamic force control method for a tilt-wing electric vertical take-off landing (eVTOL) using airflow vector estimation. With this research, the transition of an eVTOL from hover to cruise can be done more efficiently and disturbances can be controlled. R. Kowalski et al. in [25] studied a method to synthesise a force flight compensation for parallel-redundant primary flight control actuators. Research carried out by Y. Yan et al. [31] studies actuator dynamics to control a small fixed-wing UAV with direct lift control (DLC) in front of unknown external disturbances.

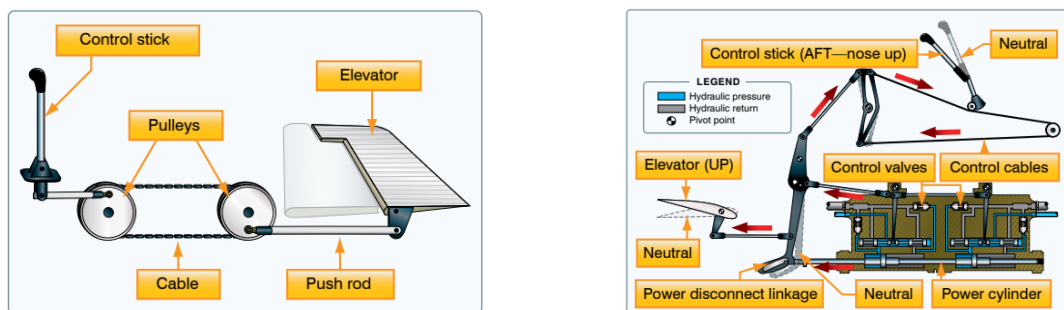
The works presented above do not achieve force control directly by delivering torque to the control surfaces. Instead, data is collected and control algorithms are developed to change the position of the actuators according to the desired force. On the other hand, work developed by Aleksey Zaitsevsky [33] introduces the concept of force servos. Which is an approach similar to the "around-the-arm". In a force servo, the force is sensed directly with a load cell and fed back to a servo motor that is providing a constant torque.

This project will study ways to sense and deliver direct force to the control surfaces rather than developing complex control algorithms that can estimate the dynamic state of the system to maintain a specific force.

2.1.1 Flight Control Systems

In the former days when the first controlled heavier-than-air aircraft was built by the Wright brothers in 1903, FCS were mechanically based, mainly, in rods, levers, cables and pulleys fig.2.1a. The maximum deflection of control surfaces to steer and manoeuvre the aeroplanes was limited by the physical strength of the pilots. Mechanical FCS are still used today in small general and sport category aircraft where the aerodynamic forces are not excessive [19].

Nevertheless, as aeroplane design evolved, larger and faster aircraft were produced. Aerodynamic forces acting upon the control surfaces grew to a point where they surpassed the limit of human strength. To enable pilots to control the aircraft, more advanced systems were needed. This way, hydro-mechanical approaches based on mechanical and hydraulic circuits were used to reduce the force required by the pilots, complexity and weight of mechanical control systems fig.2.1b. The next step was the introduction of fully power-operated controls. These are called irreversible controls since the aerodynamic hinge moment of a control surface has a minimal effect on its deflection and cannot be felt by the pilot any longer [26]. Linkages between the pilot and the hydraulic actuators were replaced by signalling. Early signals were analogue but at present with advances in electronics digital sensors such as inertial motion, pressure or air-stream direction are used. The replacement of direct linkages between pilot and control surfaces by electrical signalling is known as FBW.



(a) Mechanical flight control system.

(b) Hydro-mechanical flight control system.

Figure 2.1: Flight control systems. Extracted from p.5-2 [19].

2.1.2 Fly-By-Wire

The concept of FBW is not something which sprung up overnight, but rather it evolved slowly through the years as aircraft FCS requirements changed. With progressive increases in aircraft size and speed, power-boosted control quickly became a requirement to enable the pilot to utilize the full manoeuvre capability of the aircraft [30].

FBW has become an appropriate solution to control system issues of cutting-edge aerospace vehicles. It has enabled using aircraft configurations that were not possible before. Aircraft with low or even negative natural stability over part of the speed range of the flight envelope could rely on the FCSs to fly which provided automatic stabilisation making viable lighter and more efficient configurations compared to conventional designs. Aircraft with FBW FCS first came into service in the late 1970s using analogue implementation. Digital FBW systems have been in service since the late 1980s [18].

All new fighter designs make use of FBW control. Fig.2.2 represents the Eurofighter Typhoon as an example.

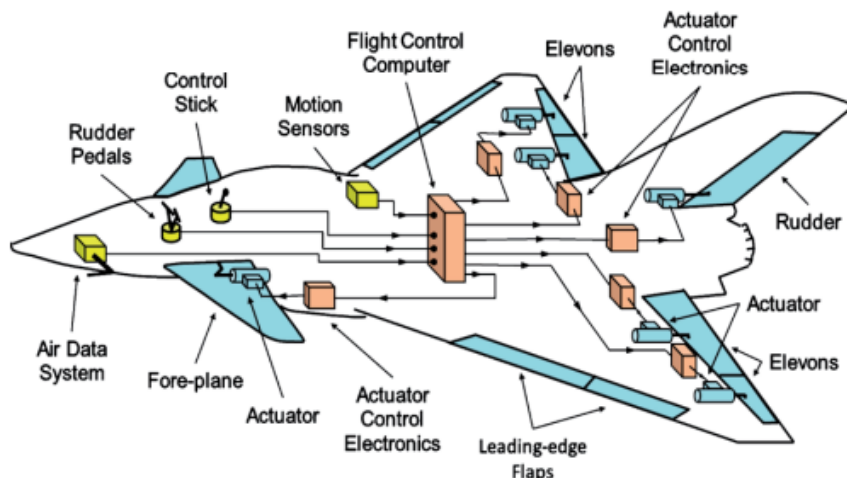


Figure 2.2: Basic elements of a fly-by-wire flight control system. [Extracted from p.180 \[18\]](#).

2.1.3 UAV Flight Control

Without the emergence of FBW technologies, the concept of UAVs would not have been possible. FCS in UAVs and manned vehicles are fundamentally the same. When it comes to piloting the vehicle, nowadays, both types of aircraft have the same control surfaces and they operate with FBW. The main difference is that in UAVs the commands are sent remotely, which allows giving them different purposes.

UAVs can be smaller than regular aircraft, can have higher range and autonomy and since UAVs do not carry human pilots, are considered to be more secure and maneuverable.

2.1.4 Flight Control Surfaces

Aircraft have multiple FCS. These surfaces allow the aircraft to be maneuverable, they can be classified in primary flight controls, meant for pitch, roll and yaw, and secondary flight control as flaps or spoilers for producing high-lift or lift-dump. By deflecting these surfaces, the pressure distribution over the airfoil changes, varying the lift and drag produced and allowing the pilot to rotate around the axis. As shown in fig.2.3 the angular speed around x axis is represented with p and the respective roll moment with L , q , and M for angular speed and pitching moment respectively for y axis and for z axis, r is the angular speed and N the yaw moment.

Civil aircraft, usually have the horizontal stabilizer positioned at the rear part of the plane. On the other hand, fighter aircraft tend to use canard configurations as they have better performance. Deflecting the canard at an angle η produces a change in pitch moment, deflecting the ailerons at an angle δ allows a rolling moment, and changing the rudder at an angle χ produces a yaw moment.

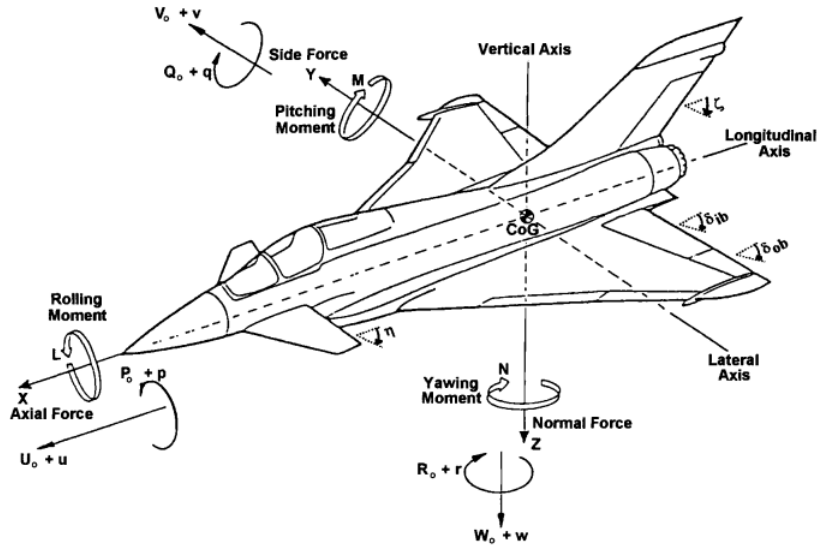


Figure 2.3: Flight control angles and moments in body frame.[Extracted from p.4 \[26\].](#)

2.1.5 Frames of reference

To describe the aircraft, a non-linear model will be presented. The navigation frame used is the North x_n , East y_n , Down z_n , where O_n is the tangent point to the earth's surfaces where the aircraft's center of gravity is located before taking off. This frame is considered inertial. The body frame is described in fig.2.3, x direction of the body frame is positive pointing forward in the longitudinal axis of the plane, y is positive along the right wing and z is normal to x , and y .

To relate the body frame and navigation frame, Euler angles are used. The navigation frame is rotated around the z axis at an angle ψ , also called yaw angle, and defines the aircraft heading. Then, this intermediate frame is rotated at an angle θ around the y axis giving the elevation or pitch angle. Finally, to obtain the roll angle ϕ , this second intermediate frame is rotated around the x axis. All the rotations are done in the positive direction of its axis. Fig.2.4 shows a 3D view of the Euler angles.

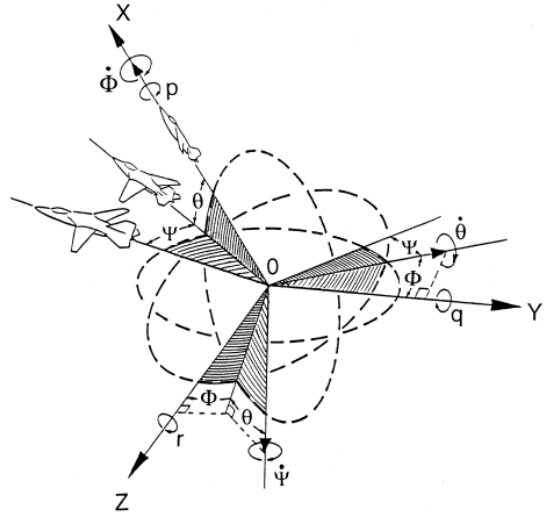


Figure 2.4: 3D representation of the Euler angles. Extracted from p.118 [18].

Hence, to change from the navigation frame A_n to the body frame A_b , the transformation matrix L_{bn} of eq.2.2 is used.

$$A_b = L_{bn} A_n \quad (2.1)$$

$$L_{bn} = \begin{pmatrix} \cos \theta & \cos \psi & \cos \theta & \sin \psi & -\sin \theta \\ \sin \phi & \sin \theta & \cos \psi - \cos \phi & \sin \psi & \sin \phi & \sin \theta & \sin \psi + \cos \phi & \cos \psi & \sin \phi & \cos \theta \\ \cos \phi & \sin \theta & \cos \psi + \sin \phi & \sin \psi & \cos \phi & \sin \theta & \sin \psi - \sin \phi & \cos \psi & \cos \phi & \cos \theta \end{pmatrix} \quad (2.2)$$

As L_{bn} is orthogonal, L_{bn}^t can be used to change from the body frame to the navigation frame. Aircraft's velocity v_b can be expressed as the sum of airspeed velocity V_T and wind velocity W_n .

$$v_b = \begin{pmatrix} u \\ v \\ w \end{pmatrix} = \begin{pmatrix} u_T \\ v_T \\ w_T \end{pmatrix} + L_{bn} \begin{pmatrix} W_x \\ W_y \\ W_z \end{pmatrix} \quad (2.3)$$

Thus, aircraft inertial velocity v , airspeed velocity V_T , angle of attack α and slide-slip angle β are defined as:

$$v = \sqrt{u^2 + v^2 + w^2} \quad V_T = \sqrt{u_T^2 + v_T^2 + w_T^2} \quad \alpha = \arctan \frac{w_T}{u_T} \quad \beta = \arcsin \frac{v_T}{V_T} \quad (2.4)$$

Considering the aircraft as a rigid body, in an inertial frame, Newton's laws of motion are expressed as.

$$\sum_j F_j = \frac{d}{dt} \Big|_i (mV) \quad \sum_j G_j = \frac{d}{dt} \Big|_i H \quad (2.5)$$

While in a non-inertial frame, as the body frame, the expressions are:

$$\sum_j F_j = \frac{d}{dt} \Big|_b (mV) + \omega_{b/i} \times mV \quad \sum_j G_j = \frac{d}{dt} \Big|_b H + \omega_{b/i} \times H \quad (2.6)$$

$$mg_b + F_b^{engine} + F_b^{aerodynamic} = m \left[\begin{pmatrix} \dot{u} \\ \dot{v} \\ \dot{w} \end{pmatrix} + \begin{pmatrix} p \\ q \\ r \end{pmatrix} \times \begin{pmatrix} u \\ v \\ w \end{pmatrix} \right] \quad (2.7)$$

$$G_b^{engine} + G_b^{aerodynamic} = \begin{pmatrix} I_x & 0 & -I_{xz} \\ 0 & I_y & 0 \\ -I_{xz} & 0 & I_z \end{pmatrix} \begin{pmatrix} \dot{u} \\ \dot{v} \\ \dot{w} \end{pmatrix} + \begin{pmatrix} p \\ q \\ r \end{pmatrix} \times \left[\begin{pmatrix} I_x & 0 & -I_{xz} \\ 0 & I_y & 0 \\ -I_{xz} & 0 & I_z \end{pmatrix} \begin{pmatrix} u \\ v \\ w \end{pmatrix} \right] \quad (2.8)$$

2.2 Control Surface Aerodynamic Analysis

There are several ways to conduct an aerodynamic analysis. As CFD methods are out of the scope of this project, an analytical analysis using lifting line theory (LLT) will be done. Nevertheless, the lower the aspect ratio the less accurate are the analytical results. This way, other numerical methods given by the software XFLR5 [8] which are based on LLT, theories will serve as a comparison.

Airfoil	S_{ref} [m ²]	b[m]	C_r [m]	C_t [m]	Λ [°]	Γ [°]	i_w [°]
NACA 64-006	0.032	0.246	0.224	0.037	34.76	0	0

Table 2.1: Canard wing geometric parameters.

2.2.1 Lift & Drag

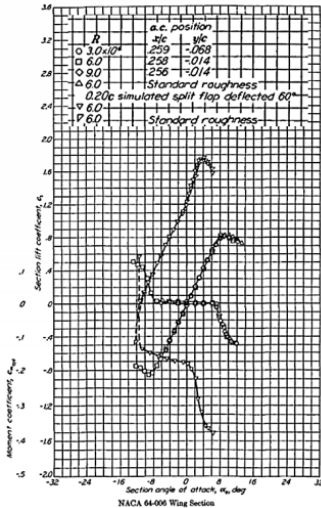
According to Prandtl LLT and Kutta–Joukowski theorem, it is known that the lift coefficient of a wing can be calculated by summing the individual circulation of each airfoil element along the wingspan. And any distribution can be expressed in terms of a trigonometric Fourier series expansion.

$$C_L = \frac{2}{SU_\infty} \int_a^b \Gamma(y) dy \quad \Gamma(\theta) = 2bU_\infty \sum_{n=1}^{\infty} A_n \sin n\theta$$

Where $A_n = \frac{2}{\pi} \int_0^\pi \frac{dz}{dx} \cos n\theta d\theta$. For trapezoidal wings eq.2.9 deduced from LLT can be used to estimate the wing's lift coefficient.

$$C_L = C_{L\alpha} \frac{AR}{2 + \sqrt{4 + AR^2}} (\alpha - \alpha_{lo}) \quad (2.9)$$

Analytical Result



From the data of fig.2.5 is known that the lift coefficient slope of the airfoil NACA 64-006 is $C_{l\alpha} = 0.109$. Then, by applying eq.2.9 the lift coefficient slope of the wing obtained analytically is $C_{L\alpha} = 0.0435$.

On the other hand, modeling the wing in XFLR5 and performing an analysis using LLT at the conditions specified by REQ-1 & REQ-2, the lift coefficient slope of the wing obtained is $C_{L\alpha} = 0.0413$, fig.2.6.

The absolute error of the lift coefficient slope between the two methods is 0.0022. Therefore, the final lift coefficient that will be assumed for the system design will be the average value between the two methods:

$$C_L = 0.0424\alpha$$

From LLT, the induced drag coefficient can be obtained with eq2.10.

$$C_{Di} = \frac{1}{\pi e AR} \quad (2.10)$$

The Oswald efficiency factor is estimated using this formula proposed in Raymer[27].

$$e = 1.78 \cdot (1 - 0.045 \cdot AR^{0.68}) - 0.64$$

$$\text{Then, } C_{Di} = \frac{1}{\pi \cdot 1.016 \cdot 1.9} = 0.165.$$

Knowing the wet wing surface, the reference surface, and the operational velocity, the parasite drag is calculated as follows. First, the Reynolds number is obtained to evaluate the skin friction coefficient. Where $l = \bar{c}$, (value calculated in next section), and ν is the dynamic viscosity of the air at 20°.

$$Re = \frac{Vl}{\nu} = \frac{41.67 \cdot 0.153}{1.516 \cdot 10^{-5}} = 4.2 \cdot 10^5$$

As the flow can be considered turbulent, the friction coefficient is estimated as

$$C_f = \frac{0.455}{(\log_{10} Re)^{2.58}(1 + 0.144M^2)^{0.65}} = 0.0053$$

Finally, the zero drag coefficient will be.

$$C_{Do} = C_f \frac{S_w}{S_{ref}} = 0.0053 \cdot \frac{0.037}{0.032} = 0.0061$$

Thus the drag coefficient that will be assumed for the system design is the following:

$$C_{Do} = 0.0061 + 0.165C_L^2$$

2.2.2 Hinge moment

As the wing is trapezoidal, the next graphic method, fig.2.7, can be used to estimate the wing's mean aerodynamic chord (MAC):

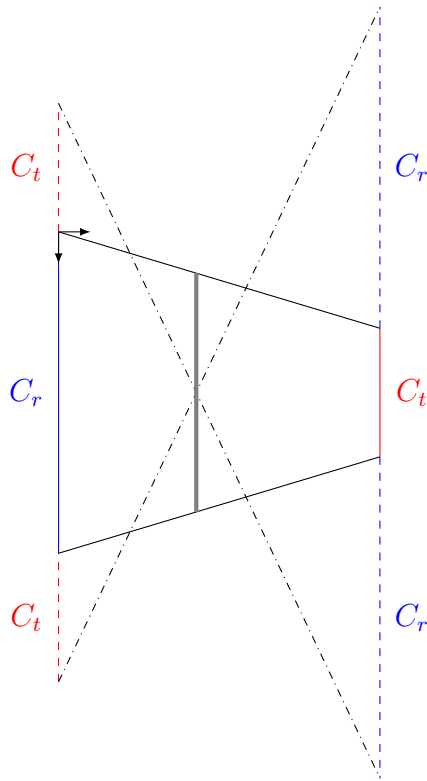
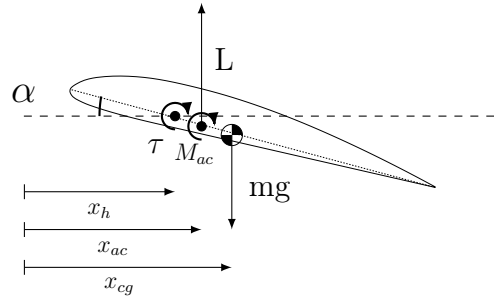


Figure 2.7: Graphic method to obtain the location of the MAC.

Therefore, $y_{ac} = 47 \text{ mm}$ and x_{ac} it is assumed to be at a quarter of the MAC which is $\bar{c} = 153.1 \text{ mm}$. Setting the reference frame at the top left edge of the semi wing the coordinates of the aerodynamic center are (88.67,47) mm.

Now that the ac is known, the stability of the wing can be studied and the hinge can be placed. To do this, the sum of momentum at the hinge is presented in eq. 2.11. It can be noticed that small angles of attack have been assumed which implies $\cos \alpha \approx 1$, $\sin \alpha \approx \alpha$.

$$\sum H_e = \tau + M_{ac} - L(x_{ac} - x_h) + mg(x_{cg} - x_h) \quad (2.11)$$



Dividing the hinge moment equation, eq.2.11, over the dynamic pressure $q = \frac{1}{2}\rho U_\infty^2$, the surface area S and the MAC \bar{c} a dimensionless hinge coefficient is obtained.

Arranging the terms, eq.2.12 is deduced.

$$C_{he} = C_{ho} + C_{h\alpha}\alpha \quad (2.12)$$

Where,

$$C_{ho} = \hat{\tau} + C_{mac} - a\alpha_o(\hat{x}_{ac} - \hat{x}_h) + \frac{mg}{qS}(\hat{x}_{cg} - \hat{x}_h)$$

$$C_{h\alpha} = -a(\hat{x}_{ac} - \hat{x}_h)$$

To achieve stability, in front of a perturbation of the angle of attack, the moment at the hinge has to oppose the change. That is to say, $\frac{\partial C_{he}}{\partial \alpha} < 0$. This way,

$$x_h \leq x_{ac}$$

To maintain a given angle of attack $\alpha = \alpha'$ in front of a variation on the dynamic pressure, the torque delivered to the hinge in equilibrium conditions will be,

$$\begin{aligned}
 \mathcal{Q}_h^0 &= \hat{\tau} + C_{mac} - a\alpha_o(\hat{x}_{ac} - \hat{x}_h) + \frac{mg}{qS}(\hat{x}_{cg} - \hat{x}_h) - a\alpha'(\hat{x}_{ac} - \hat{x}_h) \\
 \tau &= qSa\alpha_o(x_{ac} - x_h) - mg(x_{cg} - x_h) - M_{mac} + qSa\alpha'(x_{ac} - x_h) \\
 \tau &= Aq - B
 \end{aligned} \tag{2.13}$$

Being,

$$\begin{aligned}
 A &= Sa(x_{ac} - x_h)(\alpha_o + \alpha') \\
 B &= mg(x_{cg} - x_h) + M_{mac}
 \end{aligned}$$

On the other hand, if a given torque is maintained, the change of the angle of attack in front of variations on the dynamic pressure in equilibrium conditions is

$$\begin{aligned}
 C_{he}^0 &= C_{ho} + C_{h\alpha}\alpha \\
 \alpha &= \frac{\tau + M_{ac} - qSa\alpha_o(x_{ac} - x_h) + mg(x_{cg} - x_h)}{qSa(x_{ac} - x_h)} \\
 \alpha &= \frac{1}{q}C - D
 \end{aligned} \tag{2.14}$$

And,

$$\begin{aligned}
 C &= \frac{1}{Sa(x_{ac} - x_h)}(\tau + M_{ac} + mg(x_{cg} - x_h)) \\
 D &= \alpha_o(x_{ac} - x_h)
 \end{aligned}$$

Equations, 2.12, 2.13 and 2.14 are represented in fig.2.8.

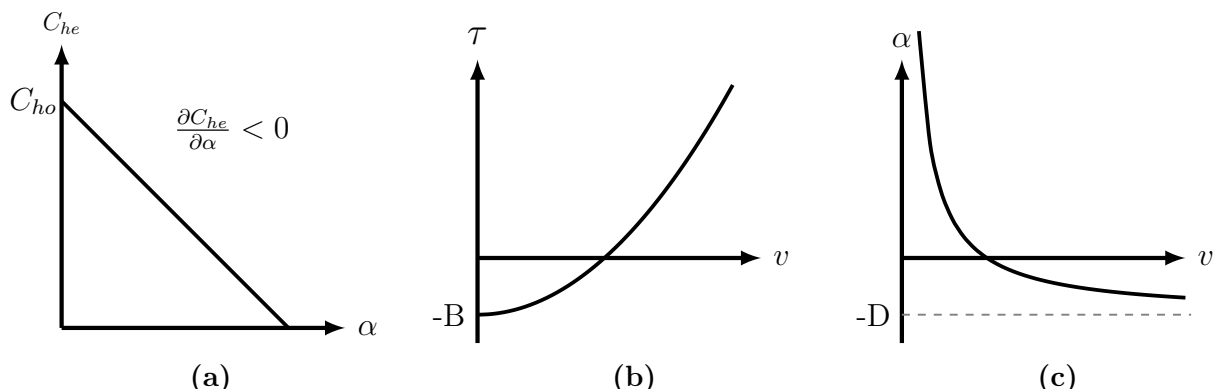


Figure 2.8: (a) Hinge moment coefficient vs alpha, (b) torque needed to maintain a specific angle of attack vs velocity, (c) for constant torque, alpha in front of velocity.

It can be noticed that the further is the hinge from the aerodynamic center, the more torque and thus, the more energy is required to control the surface.

Thus, it has been decided to place the hinge 1 cm closer to the LE than the aerodynamic center.

$$x_h = 78.67 \text{ mm}$$

To size the actuator torque, the maximum torque produced by the wing has to be determined. Unlike before, small angles of attack hypothesis can not be accepted. Therefore, the sum of moments at the hinge is:

$$\sum H_e = \tau + M_{ac} + mg \cos \alpha (x_{cg} - x_h) - L \cos \alpha (x_{ac} - x_h) - D \sin \alpha (x_{ac} - x_h)$$

$$L = qSC_{L\alpha}\alpha, \quad D = qS(CD_0 + k(C_{L\alpha}\alpha)^2), \quad M_{ac} = 0$$

The angle of attack that will produce the maximum hinge moment is derived from:

$$\frac{\partial \sum H_e}{\partial \alpha} = 0 \rightarrow \alpha_h$$

Therefore, the maximum torque applied at the hinge in equilibrium conditions, $\sum H_e = 0$, will be:

$$\tau_{max} = \frac{1}{2} \rho V_{max}^2 S (x_{ac} - x_h) [C_{L\alpha}\alpha_h \cos \alpha_h + (CD_0 + kC_{L\alpha}^2\alpha_h^2) \sin \alpha_h] - mg \cos \alpha_h (x_{cg} - x_h) \quad (2.15)$$

As α_h is out of the angle of attack range, see REQ-2. Plotting the torque function against alpha fig.2.9 it is noticed that the relative maximum and minimum angles are $\alpha_{h1} = -20^\circ$ and $\alpha_{h2} = 20^\circ$. Where $\alpha_{h1} = -20^\circ$ gives a higher absolute value of the torque.

Then, the maximum torque needed to overcome the torque produced by the whole wing in the range of angles of attack set by the REQ-2 at equilibrium condition is:

$$\tau_{max} = 3.8 \approx 4 \text{ kg} \cdot \text{cm}$$

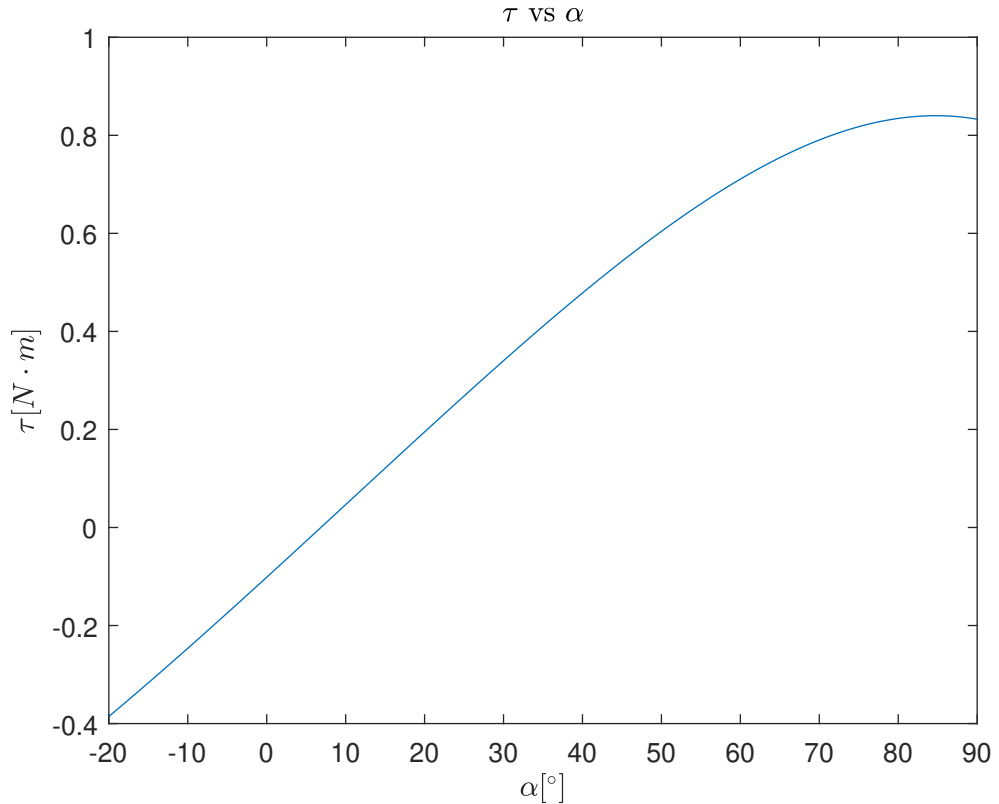


Figure 2.9: Torque produced at the hinge against the angle of attack.

MatLab script in appendix A.1

2.3 Actuators & Sensors

Actuators are devices that convert an external source of energy to mechanical energy so that a load can be moved in a controllable way, fig.2.10. Actuators come in many different shapes and sizes and can be designed to move in a linear or rotary motion. They are used in a wide range of applications, from controlling the position of an aircraft wing to adjusting the position of a robotic arm.

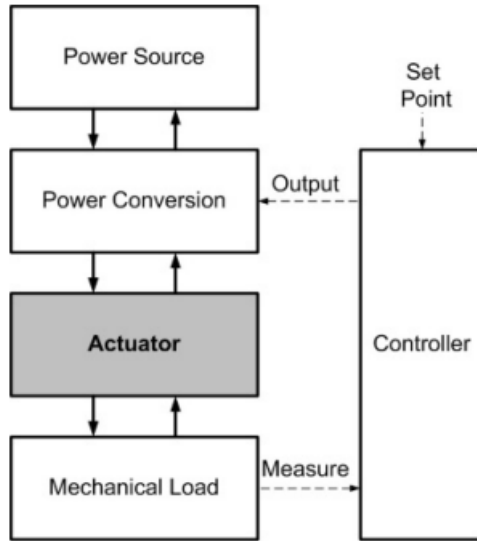


Figure 2.10: Block diagram for mechatronic systems. Extracted from p.4 [23].

Based on the physical principle of what the actuators work, different types can be distinguished.

On the other hand, sensors are defined as devices that produce an output signal for the purpose of sensing a physical magnitude. Usually, the output signal is electrical and the input magnitudes can be temperature, pressure, position, velocity, acceleration, inclination, light intensity, chemical molecules, etc.

2.3.1 Potentiometer

A potentiometer is considered an analog sensor that uses a three-terminal resistor with a sliding or rotating contact that forms an adjustable voltage divider, fig.2.11. Thanks to having a variable resistance, it can function as a position transducer.

$$V_{out} = V_{cc} \times \frac{R_2}{R_1 + R_2} \quad (2.16)$$

In this project, the potentiometer could be used to determine the position of the control surface and feed it back to a controller.

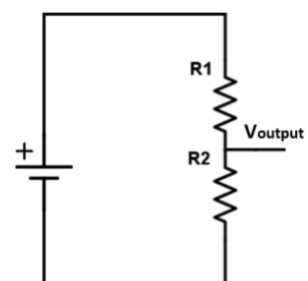


Figure 2.11: Potentiometer wiring diagram. Extracted from [15].

2.3.2 Load Cell

Load cells are considered force transducers as with the use of strain gauges they can measure the force applied in a load. For this project, having a reading of the force produced could be useful in closed-loop control. Strain gauges are usually placed in a Wheatstone bridge to measure the relative change in resistance, fig.2.12. Several configurations can be used, considering a full bridge, that is to say, a Wheatstone bridge where all the resistors are strain gauges placed with the same orientation in a rectangular beam on each face, strain can be expressed as stated in eq. 2.17. Where k is an intrinsic factor of the gauge.

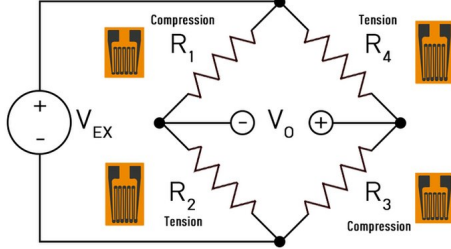


Figure 2.12: Full Wheatstone bridge.
Extracted from [6].

$$\epsilon = \frac{1}{k} \frac{V_0}{V_{EX}} \quad (2.17)$$

2.3.3 Electromechanical Actuators

Electromechanical actuators (EMAs) produce force or torque converting magnetic or electric energy into mechanical motion. Electric motors are considered EMAs as they make use of electromagnetism to produce mechanical movement. Most electric motors work by electromagnetism, but motors based on other electromechanical phenomena, such as electrostatic forces and the piezoelectric effect, exist as well.

Rotatory motors can be classified as direct current (DC) motors or alternating current (AC) motors. DC motors have coils laying in the magnetic field of permanent magnets and a commutator reverses the direction of the electric current twice in every cycle to produce a constant revolution speed and torque. AC motors make use of the difference between the three phases to create a rotatory electromagnetic field inside the motor this way, conductors embedded in steel at the center of the motor experience an induction force that produces a rotatory motion.

The torque produced by a conventional DC motor can be expressed as:

$$T = K_T \Phi I \quad (2.18)$$

Where K_T is a constant for a given motor, Φ is the total magnetic flux, and I_m the current supplied to the motor. As the magnetic flux can be considered constant eq.2.18 can be rewritten as $T = k_t I$ being $k_t = K_T \Phi$.

Two particular kinds of electric motors, besides from conventional AC and DC, which could be used to attain the aim of this project, are brush-less direct current motors (BLDCM), fig.2.13, and servo motors, fig.2.14.

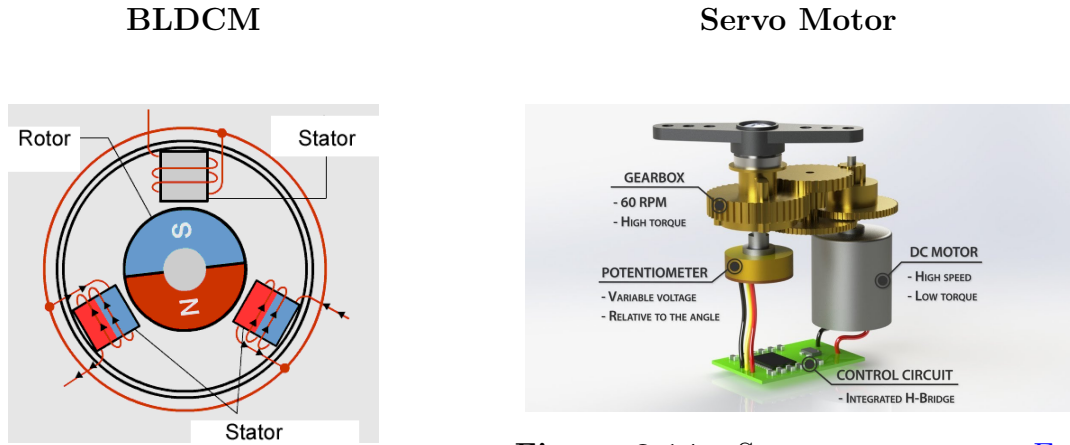


Figure 2.13: BLDCM diagram. Extracted from [1].

Unlike conventional DC motors, BLDCMs are electronically commuted. They use an electronic controller which switches DC current to the different motor windings. This produces a magnetic field that is followed by permanent magnets attached to the rotor. By adjusting the frequency and amplitude of a pulse width modulation (PWM) signal sent to the electronic controller, speed and torque can be adjusted.

Another variation of servo motors worth mentioning is **Force Servo**. A force servo can be defined as a servo motor that includes a force measurement in the feedback loop. This can be done in different ways. As mentioned in 2.1, Aleksey Zaitsevsky developed a force servo by using a force transducer that transforms strain to an electric signal using strain gauges [33]. A control surface model that uses a force servo built by Aleksey Zaitsevsky has been developed by the FLUMES department. With this technique, force control is achieved, nevertheless, the torque produced is not enough to fulfill the requirements and the behavior is not linear.

To handle the control surfaces, EMAs work in conjunction with gears, nuts, screws, and bearings as can be observed in fig.2.15.

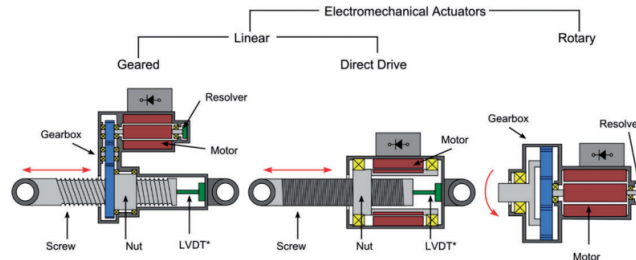


Figure 2.15: EMA for the MEA. Extracted from [21].

Figure 2.14: Servo motor parts. Extracted from [7].

Servo motors are very similar to conventional AC or DC motors, what sets them apart from regular motors is the feedback loop and drive system. These motors have a sensor that reads the motor's position, it could be an encoder, resolver, or a potentiometer. Then, this information is fed to the drive unit and the position can be controlled. In addition, a set of gears is placed to achieve the desired torque-rpm ratio.

2.3.4 Fluid power actuators

Fluid power actuators make use of fluid properties to produce mechanical work. If the fluid is in-compressible the actuators are classified as hydraulic actuators, otherwise, compressible fluids are classified as pneumatic actuators.

Both hydraulic and pneumatic actuators have their own advantages and drawbacks. Some of them are quoted in table 2.2. These types of actuators can be an adequate option for force control as they work by producing either a pressure or a surface difference between chambers that give a constant force, see fig.2.16.

$$F = PS \quad (2.19)$$

$$\Delta F = F_1 - F_2 = D_1 P_1 - (D_1 - D_2) P_2 = ma$$

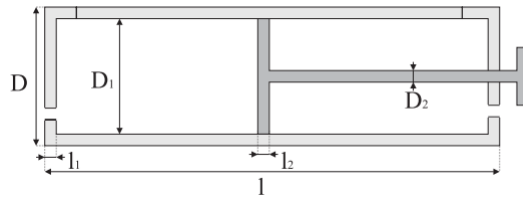


Figure 2.16: Geometry of hydraulic actuator. [Extracted from p.134 \[23\]](#).

Hydraulic	Pneumatic
Advantages	
Easily controllable	Easily controllable
Very high force	High force
Good lifetime	Moderate lifetime
Fast	Very fast
Long strokes (if needed)	Long strokes (if needed)
Drawbacks	
Flow leakage	Flow leakage
Low efficiency	Low efficiency
Inflammable oils	Medium/Low position accuracy
Relatively heavy	High noise levels

Table 2.2: Advantages and drawbacks of Hydraulic and Pneumatic actuators.

In general aviation, hydraulic actuators (HA) are widely used. Fig.2.17, shows a simplified scheme of a HA used to control a control surface. Conversely, is harder to find small fixed-wing UAVs using HA.

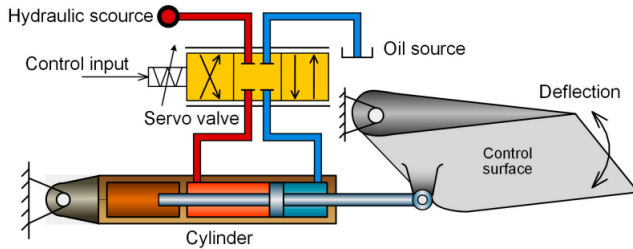


Figure 2.17: The typical structure of the HA system. Extracted from [29].

2.4 Control

Control theory is a branch of engineering and applied sciences that studies how to control dynamic systems. Its main objective is to develop models and algorithms based on the system's physical properties to drive it to a desired state. A control model or algorithm is considered adequate when the delays, steady-state errors or overshoots are minimized while the stability is assured.

The object to be controlled (the canard wing in this project) is referred to as the plant, while the process that sets the control is named as controller. Both plant and controller are a set of self-defined physical bodies under study, that make a control system.

Two main types of control strategies can be distinguished.

- **Open-loop control systems** are control systems that operate without feedback. They use predetermined inputs to produce a fixed output. The system does not monitor the output to adjust the input, so it can be less accurate and prone to errors.
- **Closed-loop control systems**, also known as feedback control, are control systems that use feedback to adjust the output of the system. The system continuously monitors the output and adjusts the input to achieve the desired output. This type of control is more accurate and reliable than open loop control because it takes into account the system's response to its input.

2.4.1 Electronic Speed Control

As BLDCMs may be used to reach the objective of this project, it is worth reviewing how speed and torque control is done.

An electronic speed controller (ESC) is an electronic circuit made of Metal Oxide Semiconductor Field-Effect Transistors (MOSFETs) which act as electronic commutators to deliver current to the three phases, A, B, and C of a BLDCM, see fig.2.18. The switching frequency of the MOSFETs is translated to rotational speed in the motor. This frequency can be controlled with various protocol signals being PWM the most common. The PWM is usually generated with a microcontroller. By increasing the voltage of the signal, torque is increased.

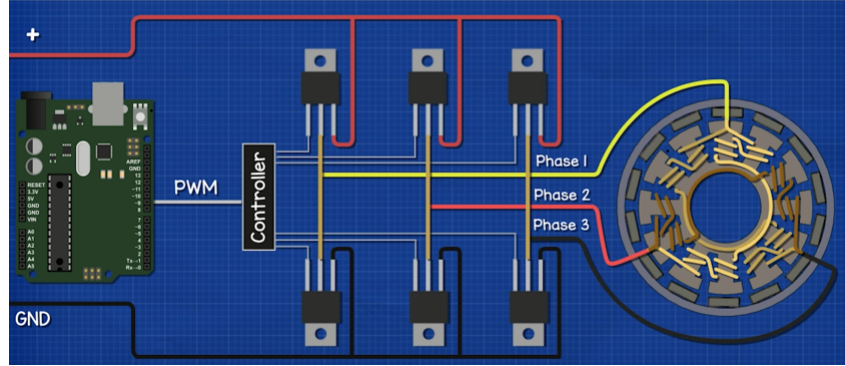


Figure 2.18: ECS schematic. Extracted from [3].

Electronic speed control can be achieved within open-loop control. Different computation methods can be applied to control the BLDCM.

► Trapezoidal Commutation

This commutation method is relatively easy to implement. It can produce high torque and speed while maintaining low switching losses. As shown in fig.2.19, there are six possible states in which each phase is high, low, or in transition. [24]

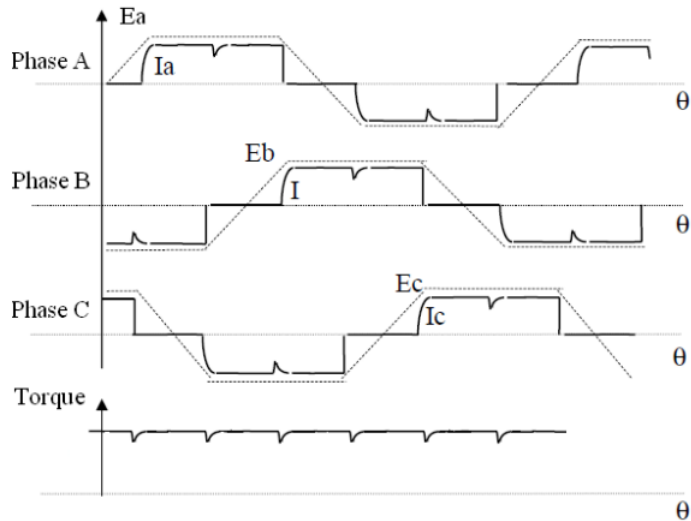


Figure 2.19: Trapezoidal commutation. Extracted from[24].

At each phase transition, it can be noticed a torque ripple at each 60 degree phase commutation due to the change in frequency which leads to audible noise and not maximizing the motor's efficiency.

► Sinusoidal Commutation

The goal of this commutation method is to achieve output currents for each phase that are sinusoidal. This is achieved by changing the duty cycle of the PWM signal,

see fig.2.20. Sinusoidal commutation allows higher efficiencies, lower audible noise, and low torque ripples for stable loads. Nevertheless, each phase will require a PWM control, producing more switching losses, and torque ripple is produced for dynamic loads when the speed is changing.



Figure 2.20: Sinusoidal pulse width modulation. Extracted from [24].

► Field Oriented Control

Field oriented control (FOC) also known as vector control was originally developed for motor applications that required to operate smoothly over full speed range, generate full torque at zero speed, and have fast accelerations.

In FOC a sinusoidal PWM (SPWM), is also used to excite the three phases with a sinusoidal current that is 120° apart from each phase and creates a rotating magnetic field in the stator. The maximum torque is achieved when the rotor's magnetic field is 90° apart from the stator's field, fig.2.21. Hence, the rotor's position is measured with magnetic encoders such as Hall effect sensors, measuring the back electromagnetic force of the three phases or other types of encoders as incremental or absolute. This information is fed back in closed-loop control to assure orthogonality between the rotor's and the stator's magnetic fields.

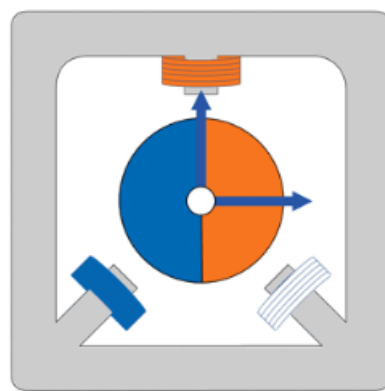


Figure 2.21: Rotor's and stator's magnetic field. Extracted from [4].

2.4.2 Encoders

An encoder is an electromechanical device that provides an electrical signal that is used for speed and/or position control. Encoders turn mechanical motion into an electrical signal that is used by the control system to monitor specific parameters of the application and make adjustments if necessary to maintain the machine operating as desired. There are several types of encoders such as incremental or absolute, optical or magnetic, shafted or hub/hollow shaft, among others.

Incremental encoder

An incremental encoder has two output signals, A and B, which issue pulses when the device is moved, see fig.2.22. Together, the A and B signals indicate both the occurrence of and direction of movement.

Unlike an absolute encoder, an incremental encoder does not indicate absolute position it only reports changes in position and, for each reported position change, the direction of movement. Consequently, to determine the absolute position at any particular moment, it is necessary to send the encoder signals to an incremental encoder interface, which in turn will track and report the encoder's absolute position. Incremental encoders report position changes almost instantaneously, which allows them to monitor the movements of high-speed mechanisms in near real time. Because of this, incremental encoders are commonly used in applications that require precise measurement and control of position and velocity [5].

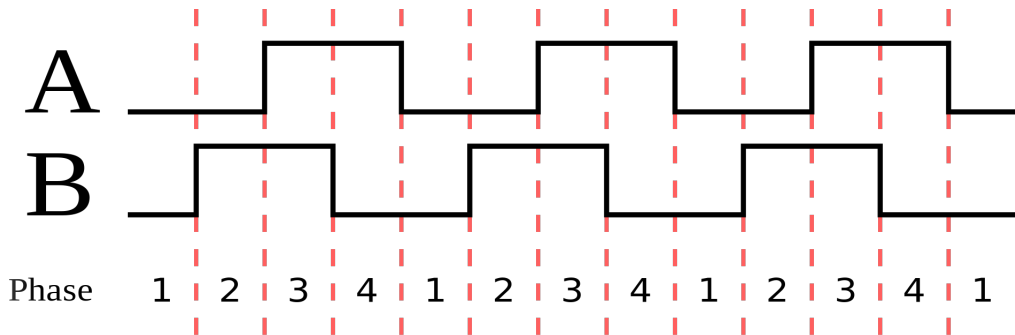


Figure 2.22: Incremental encoder signal combinations. Extracted from [5].

Magnetic encoder

The magnetic encoder uses a series of magnetic poles to represent the encoder's position to a magnetic sensor. The magnetic sensor reads the magnetic pole positions. This code can be read by a controlling device, such as a microprocessor or microcontroller to determine the angle of the shaft, similar to an optical encoder. The absolute analog type produces a unique dual analog code that can be translated into an absolute angle of the shaft. Due to the nature of recording magnetic effects, these encoders may be optimal to use in conditions where other types of encoders may fail due to dust or debris accumulation. Magnetic encoders are also relatively insensitive to vibrations, minor misalignment, or shocks [5].

Chapter 3

Concept Generation, Evaluation & Development

In this third chapter, four conceptual designs to achieve force control are presented. The first one is based on measuring the elongation of a spring and translating it into a force measurement. The second one follows the same philosophy as the former, nevertheless, force input is measured with electric force transducers as strain gauges. For the last two concepts, a different approach is reached. Force is controlled directly by regulating the current or voltage a motor receives and therefore the torque it delivers. To end with this chapter, a comparison and evaluation between concepts is presented. The most promising ones are developed in more detail.

3.1 System Development Process

In order to conduct the preliminary designs, the methodology followed is the one proposed by Roger W. Pratt fig.3.1.

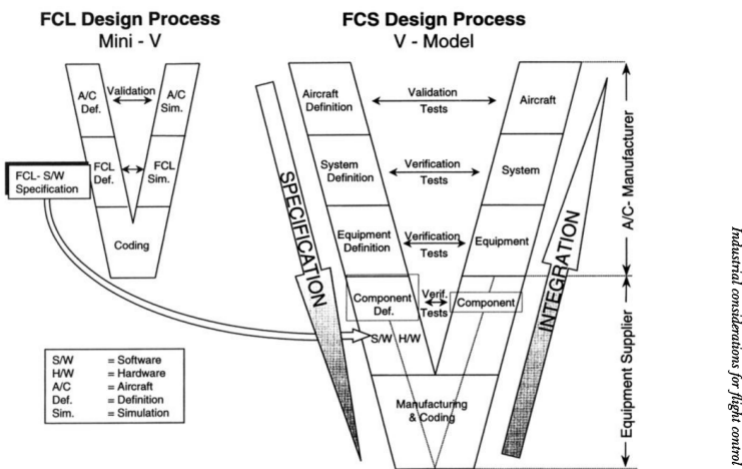


Figure 1.17 FCS design process as defined by the V-model

Figure 3.1: FCS design process as defined by the V-model. Extracted from p.45 [26].

It consists of a V-model, analytical steps are depicted on the left leg, and synthesis steps are on the right leg. Specifications increase from top to down, until reaching Manufacturing & Coding. Integration starts from the last point until reaching complete implementation in the aircraft. As the integration of the system is out of the scope of this project only the left leg of the V-model will be followed.

This chapter will be focused on explaining the concepts and defining the equipment and components needed to build two of them.

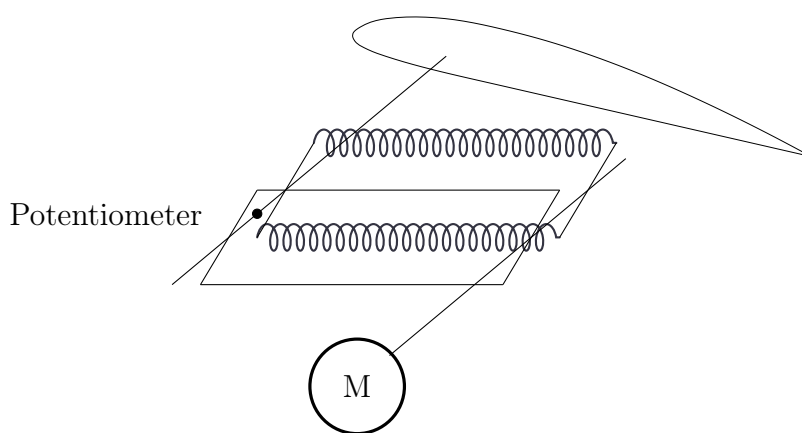
3.2 Force Transducers

As has been mentioned in section 2.3, force transducers can be defined as devices that convert a force input into an electrical output signal. With this methodology, two designs are presented. One uses springs to measure the force, and the other uses strain gauges to measure strain and consequently force.

3.2.1 Concept 1

This first concept, makes use of a potentiometer to measure the deflection between two levers attached to two different shafts. The inner left shaft is connected to the wing. The inner left lever has two springs at each end linked to another lever attached to a motorized shaft (right shaft). The outer left lever, has two cables at each end linked to another lever attached to the same motorized shaft, fig.3.2.

As the cables can be considered to maintain a constant length, by measuring the angular deflection between outer and inner left shafts and by knowing the spring constant k a reading of the force delivered to the wing is achieved. Then, feeding back the force to the motors, force control is accomplished.



Material	Units
Cable	2
Lever	4
Servo Motor	1
Potentiometer	1
Rod	3
Spring	2

Table 3.1: Materials for concept 1.

Figure 3.2: Concept 1, simplified scheme.

Advantages	Drawbacks
Lightweight	Moving parts
Simple	Multiple points of failure
Easy to maintain	Noise
Cheap	Possible oscillations

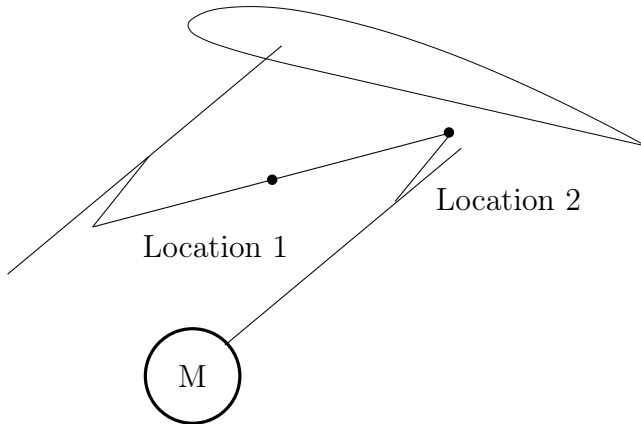
Table 3.2: Concept 1, advantages and drawbacks.

3.2.2 Concept 2

For the second concept, force is measured by a load cell. The load cell can be placed in several locations. Two locations are proposed, fig.3.3:

- **Location 1:** Place the load cell in between the rod that translates the movement between the motorized shaft and the hinge rod. Hence, with the load cell tension and compression can be measured.
- **Location 2:** An alternative placement, would be putting the load cell at the lever linked to the motorized shaft. With this configuration, the bending moment could be measured and translated to a force.

In addition, for both scenarios, a signal amplifier is needed to read the voltage of the load cell, as it delivers a low-amplitude signal. Afterwards, this signal can be fed back to the motor to reach force control.



Material	Units
Lever	2
Load cell	1
Servo Motor	1
Rod	3

Table 3.3: Materials for concept 2.**Figure 3.3:** Concept 2, simplified scheme.

Advantages	Drawbacks
Lightweight	Moving parts
Simple	Multiple points of failure
Easy to maintain	Noise in voltage signal
Less moving parts	Expensive

Table 3.4: Concept 2, advantages and drawbacks.

3.3 Pressure Control

An alternative way to attain force control is by regulating the pressure in fluid-powered actuators. Some of the basic principles of these actuators are studied in section 2.3.4. In general aviation HAs are commonly used due to some of the advantages quoted in table 2.2. On the other hand, for small UAVs the use of fluid power actuators is not common because of their weight, leakage, and low efficiencies. Therefore, is hard to find in the market small hydraulic or pneumatic actuators suitable for designing FCSs for a UAV.

This way, for this project, pressure control is discarded.

3.4 Direct Motor Control

The last approach proposed to have force control is by regulating directly the motor. Unlike the last two approaches, where external inputs such as deflection angle or strain were fed back to the motor, for this approach intrinsic characteristics such as motor current, voltage, or rotor's position are used to control the motors.

3.4.1 Concept 3

The third concept will make use of a servo amplifier to regulate the current delivered to a brushed DC motor. The transfer function of a DC is shown in fig.3.4.

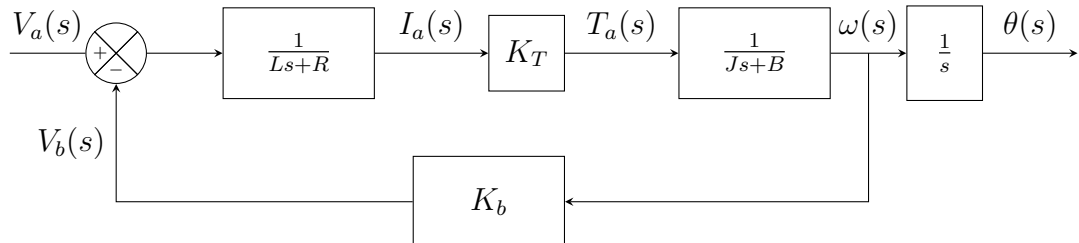


Figure 3.4: DC motor block diagram.

In this model, the input is a voltage and the output is the angular position. To control the current, last transfer function can be rearranged as in fig.3.5.

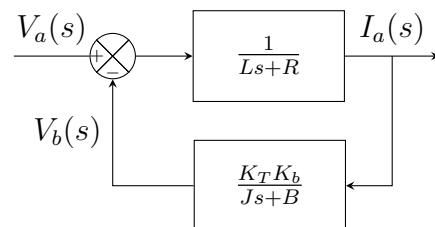


Figure 3.5: Reduced DC motor block diagram.

As the change of current is much faster than the change of speed. The block on the feedback path can be considered as a disturbance and the final transfer function is as expressed in fig.3.6:

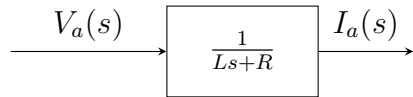


Figure 3.6: Simplified DC motor block diagram.

To achieve zero error at a steady state a proportional-integral (PI) controller is needed, fig.3.7.

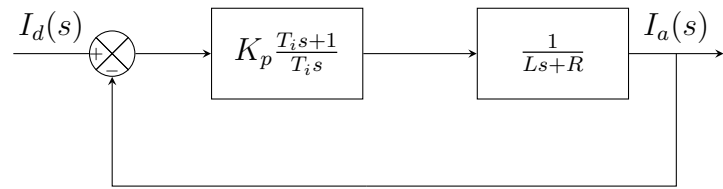


Figure 3.7: Closed loop control diagram of DC motor.

Thus, by adjusting the proportional constant K_p and the integral time constant T_i , the current can be controlled. Given a maximum overshoot m_p and maximum response time T_r . K_p has to be:

$$K_p = \frac{T_i \sqrt{R^2 - 2RL\xi\omega_n + L^2\omega_n^2}}{\sqrt{1 - 2T_i\xi\omega_n + T_i^2\omega_n^2}} \quad (3.1)$$

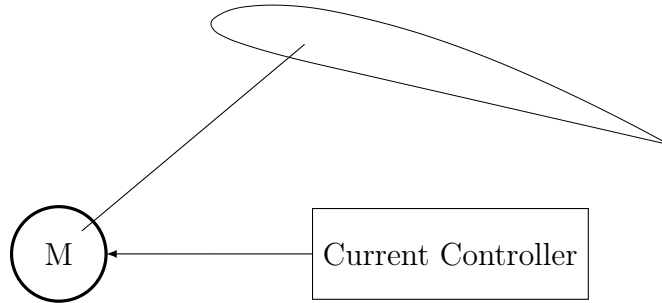


Figure 3.8: Concept 3, simplified scheme.

Advantages	Drawbacks
Less moving parts	Motor cogging
Lightweight	Wear on brushes
Simple	Un-tuned controller
Easy to maintain	Less cheap

Table 3.5: Concept 3, advantages and drawbacks.

Material	Units
Current controller	1
Brushed DC Motor	1
Rod	1

Table 3.6: Materials for concept 3.

3.4.2 Concept 4

For the fourth concept instead of using a brushed DC motor and regulating its voltage, the torque and position of a BLDCM are adjusted using FOC.

The particular BLDCM proposed for this concept is a gimbal motor. These types of motors are good holding torque, they have much larger resistance and inductance compared to usual BLDCM, nevertheless, they provide a smooth motion with low currents. They are usually used for camera stabilization.

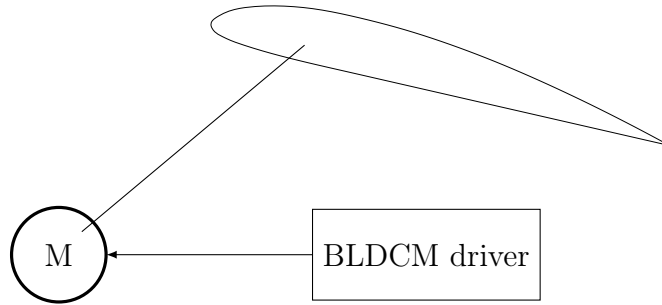


Figure 3.9: Concept 4, simplified scheme.

Advantages	Drawbacks
Less moving parts	Higher weight
High efficiencies	Less simple
Smooth motion	Electromagnetic interference EMI
Easy to maintain	Less cheap

Table 3.7: Concept 4, advantages and drawbacks.

Material	Units
BLDCM	1
BLDCM driver	1
Rod	1

Table 3.8: Materials for concept 4.

3.5 Concept Evaluation

To start with the equipment definition phase, as depicted in fig.3.1, at least one of the concepts has to be selected. As the concepts are not completely developed it is hard to make an accurate comparison between them. The method proposed to select a concept is the Ordered Weighted Average (OWA).

3.5.1 Ordered Weighted Average

In this OWA, several qualitative and quantitative criteria as simplicity or volume are weighted between 1-10, that is to say, $g_i \in [1, 10]$. Then each concept is evaluated according to the criteria between 1-5, $p_i \in [1, 5]$. Finally, applying formula 3.2 at each option. The OWA score is calculated. The higher the OWA score, the better the option.

The criteria that will be assessed are the following. It is worth mentioning that, even though there are quantitative criteria such as the occupied volume or power consumption,

all the criteria will be considered qualitative because at this stage of the conceptual design quantitative date is still unknown.

- **Volume:** As the force control system is intended to be implemented in the fuselage of an aircraft, the lower the volume the better.
- **Mass:** To be more efficient and increase the payload, the lower the mass the better.
- **Power consumption:** For the same reasons as before, the lower the power consumption the better.
- **Robustness:** Robustness is defined as the ability of the system, to perform consistently and reliably in front of variations, uncertainties, or perturbations. The more robust the system the better.
- **Moving parts & Simplicity:** Having fewer moving parts and a simple concept allows lower costs of maintenance and presents fewer points of failure.
- **Price:** Due to the limited budget of the project, the lower the price the better.

$$OWA = \frac{\sum_{i=1}^n p_i \cdot g_i}{p_{max} \sum_{i=1}^n g_i} \quad (3.2)$$

CRITERIA	Weight	Concept 1	Concept 2	Concept 3	Concept 4
Volume	g 7	p 1	gxp 7	p 3	gxp 21
Mass	8	3	24	3	24
Power consumption	8	4	32	4	32
Robustness	9	2	18	4	36
Moving parts & Simplicity	6	1	6	3	18
Price	4	5	20	2	8
SUM	42		107		139
OWA		0,51		0,66	0,74
					0,79

Table 3.9: OWA of design concepts.

Therefore, according to the OWA method, the best concept is **Concept 4**.

3.5.2 Additional Evaluations

Concept 4 seems to be the most promising. It allows to attain force control using a BLDCM which is highly efficient, provides a smooth motion, is easy to maintain, and has few moving parts. The main complexity of this concept is to implement FOC in closed-loop control using the information of a magnetic encoder. In addition, having high-frequency rotating magnetic fields in the motor's stator, ECS and magnetic encoder could produce electromagnetic interferences (EMIs) with other avionic equipment in the UAV.

For this reason, it is thought that, even though concept 1 has obtained the lowest score in the OWA, it could be worth exploring given its low price and its relatively simple working principles. Furthermore, it is known that similar mechanisms as those used in Concept 1 have been already successful to achieve force control.

3.6 Concept Development

Thus, **concepts 1 and 4** are going to be further developed.

3.6.1 Working principles

Concept 1

The force produced by the springs can be obtained as a function of the servo deflection angle θ and the analog read of the potentiometer x which is translated to an angle ϕ . That is to say, $F(\theta, \phi)$.

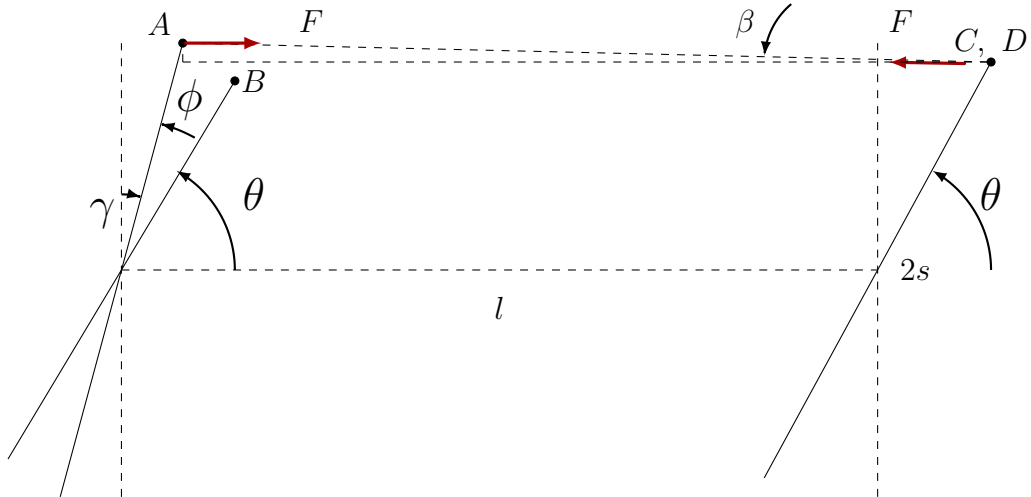


Figure 3.10: Concept 1, 2D geometric scheme.

The two right levers of distance $2s$, share the same motorized shaft which can be deflected at an angle θ . The left two levers are attached to two different rods, the inner rod is the wing's hinge. In between the two rods, a potentiometer is placed. This potentiometer measures the angle ϕ , which equals to $\phi = 90 - \theta - \gamma$. Being, θ the angle of the servo motor and ϕ , the pitch angle of the wing. Phi will be obtained as an analog signal from a microcontroller like an Arduino UNO.

Let's say that 5 V are applied to the potentiometer, and it can turn up to 285° . If the micro-controller reads 1 V that means, the potentiometer has been deflected $\frac{1}{5} \frac{V}{V/285^\circ} = 57^\circ$. In the Arduino environment, the analog signal from the potentiometer is converted to a 10 bit number going from 0 to 1023. Knowing the angle range of the potentiometer, this 10 bit number can be converted to an angle using the map function.

As the outer levers are linked with cables at both ends, distance \overline{BC} is constant and equals to l . On the other hand, inner levers are linked with springs of an initial longitude $l_0 = l$. Points A and D and distance \overline{AD} are:

$$A(s \cos(\theta + \phi), s \sin(\theta + \phi)), D(l + s \cos \theta, s \sin \theta)$$

$$\overline{AD} = \sqrt{(l + s \cos \theta - s \cos(\theta + \phi))^2 + (s \sin \theta - s \sin(\theta + \phi))^2}$$

Therefore, the force produced by one spring is:

$$F(\theta, \phi) = k \cdot (\sqrt{(l + s \cos \theta - s \cos(\theta + \phi))^2 + (s \sin \theta - s \sin(\theta + \phi))^2} - l) \quad (3.3)$$

Being k the spring constant. The torque at the hinge will be:

$$\tau = 2sF \cos(90^\circ - \phi - \theta - \beta) \quad (3.4)$$

Where β :

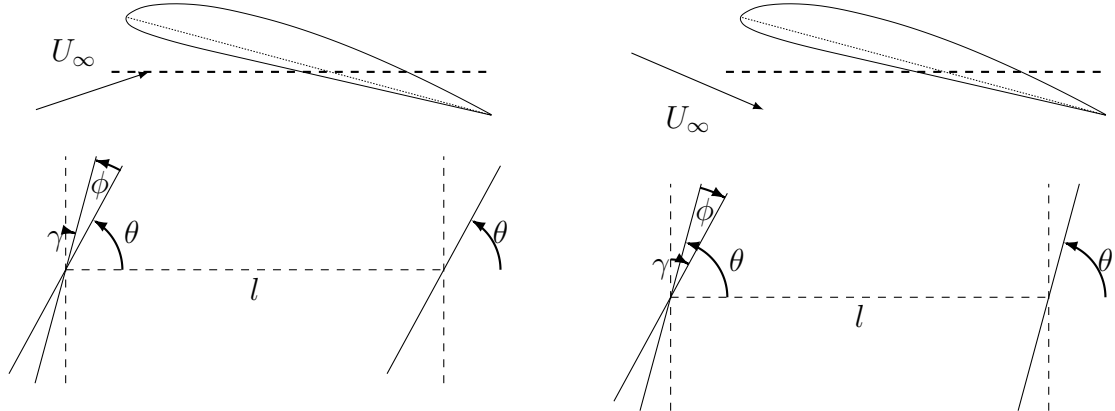
$$\beta = \arctan\left(\frac{s \sin(\theta + \phi) - s \sin \theta}{l + s \cos \theta - s \cos(\theta + \phi)}\right) \quad (3.5)$$

Four case scenarios, with positive and negative combinations of θ and ϕ can be distinguished:

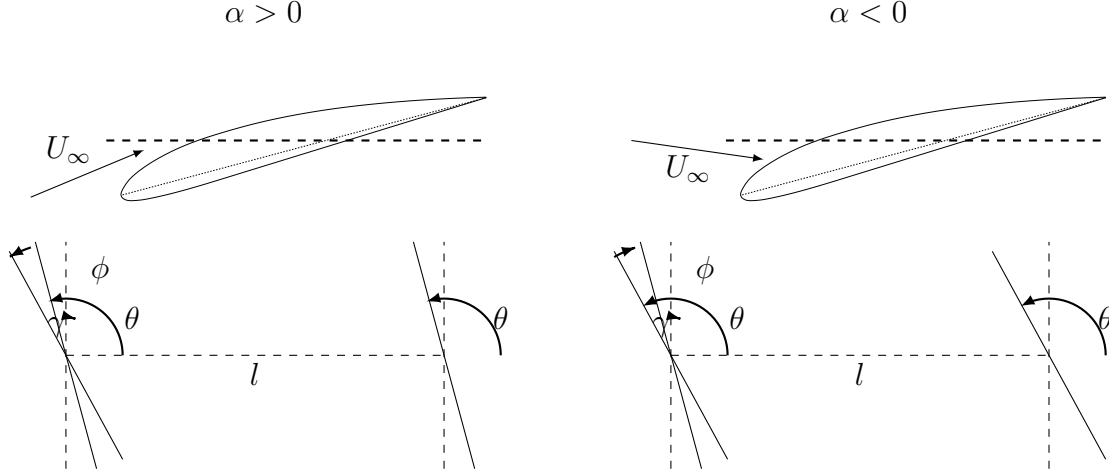
Positive pitch angle

$$\alpha > 0$$

$$\alpha < 0$$

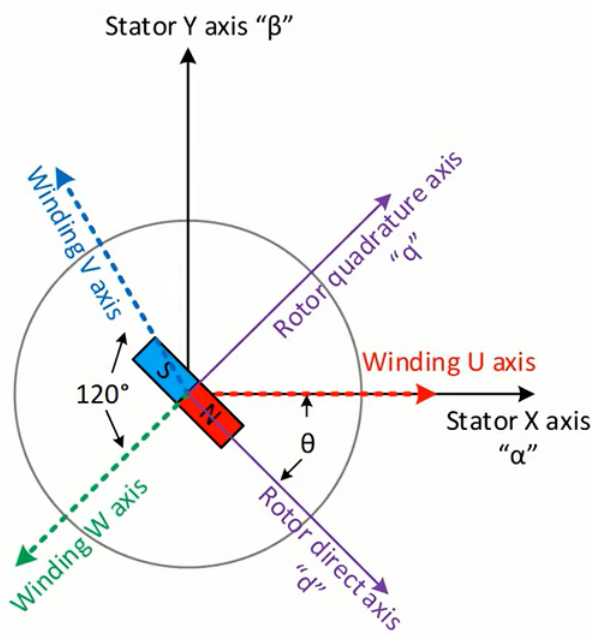


Negative pitch angle



Concept 4

In this concept, the torque is delivered to the shaft directly by a gimbal motor. The biggest challenge lies in delivering a constant torque without magnet cogging. This will be achieved using FOC, which works as follows.



The phase currents will be called I_U , I_V and I_W which are separated 120° in a three phase system.

A fixed XY coordinate system is defined and referred to as α and β . The three current phases can be projected in the $\alpha - \beta$ axis using the Clarke transform equations to obtain I_α and I_β . Finally, direct and quadrature vectors are defined. The direct component d is aligned with the rotor magnetic field, the quadrature component is perpendicular to the direct, and the angle θ separates the rotor's and stator's positions. To obtain I_d and I_q , I_α and I_β are projected in the $d - q$ axis using the Park transform equations.

Figure 3.11: Rotor and stator magnetic fields. Extracted from [24].

Clarke transform equations

$$I_U, I_V, I_W \rightarrow I_\alpha, I_\beta$$

$$\alpha = U + V \cos 120 + W \cos 240$$

$$\beta = V \sin 120 + W \sin 240$$

$$\alpha = U - \frac{1}{2}V - \frac{1}{2}W \quad \beta = \frac{\sqrt{3}}{2}V - \frac{\sqrt{3}}{2}W \quad (3.6)$$

Park transform equations

$$I_\alpha, I_\beta \rightarrow I_d, I_q$$

$$d = \alpha \cos \theta + \beta \sin \theta, \quad q = \alpha \sin \theta + \beta \cos \theta \quad (3.7)$$

The motor control system is represented in fig.3.12.

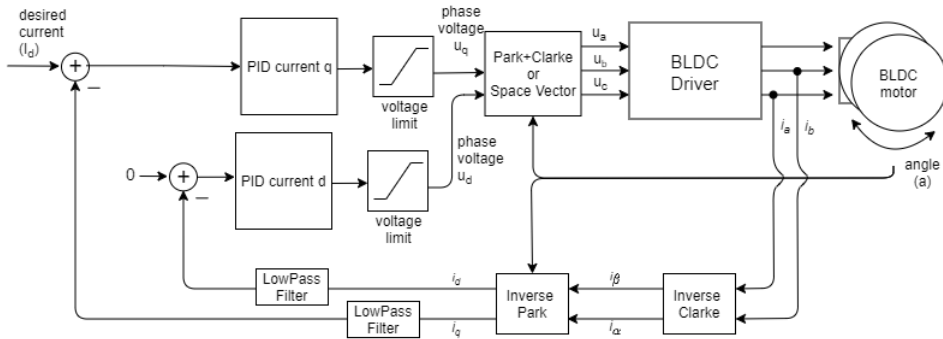


Figure 3.12: FOC implementation block diagram. Extracted from [16].

Measuring the rotor's position with an encoder and knowing the three-phase currents, Clarke and Park transform equations can be applied to obtain I_d and I_q . Then, with a PI torque controller I_q can be maximized and I_d minimized. The loop is closed when the inverse Park and Clarke transforms are applied to send a PWM signal that drives the motor.

With this strategy, as the rotor angular position θ is constantly measured, the field remains perpendicular to the current, torque is maximized and cogging is avoided. Thus, by changing the current value, torque is controlled and force control is attained. With the open-source SimpleFOC project [2], this technique will be implemented.

3.6.2 Equipment Definition & Sizing

Concept 1

To build concept 1, the following components are needed:

1. Servo motor

The servo motor will control the deflection angle θ . In section 2.2.2 it has been calculated that the maximum torque produced at the wing's hinge is $4 \text{ Kg} \cdot \text{cm}$. Nevertheless, the servo motor is not located at the wing's hinge, instead, it is within a distance l . The direction of the force applied by the springs will not be always perpendicular to the inner left lever. Thus, a servo motor capable of providing more than $4 \text{ Kg} \cdot \text{cm}$ is required. Furthermore, the servo motor shall operate between 6-8 V, as established in REQ-4. Thus, MKS DS6630 servo motor, fig.3.13, has been selected due to its torque, power, improved stability, and durability.

MKS DS6630 Specifications		
	Voltage [V]	
	4.8	6
Torque [Kg·cm]	3.61	4.7
Speed [sec/60°]	0.13	0.09
Weight [g]	28	

Table 3.10: MKS DS6630 specifications.



Figure 3.13: Servo motor MKS DS6630 [13].

This servo motor can turn up to 360° . And its dimensions are 35.8 x 15.2 x 29 mm.

2. Micro-controller

The microcontroller will command the angular position of the servo motor to reach a small force error in a steady state. This is achieved by measuring the angle of the potentiometer ϕ and the angular deflection of the servo motor θ . There are several microcontrollers available in the market. As an Arduino UNO, fig.3.14, was available at FLUMES department it will be used.

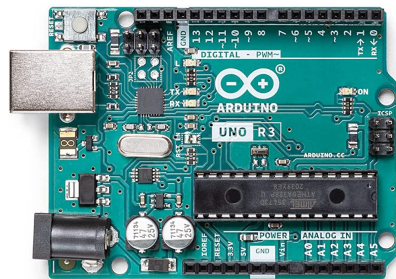


Figure 3.14: Arduino UNO board [9].

Arduino Uno is a microcontroller board based on the ATmega328P. It has 6 analog inputs and several PWM output ports which are more than enough for this project.

3. Potentiometer

The main function of the potentiometer is to measure the angle between the spring lever (inner left) and cable lever (outer left), ϕ . As the potentiometer only functions as a variable voltage divider, which analog signal is then converted to a digital 10 bit number by the Arduino board, any resistance value could be used. For the Arduino UNO, resistance values between 1 – 50 k Ω are recommended. As the potentiometer will have 5 V applied and the dissipated power equals to $P = V^2/R$ the higher the resistance the lower the losses. Therefore, the potentiometer shown in fig.3.15 is chosen.

P11S1V0FLSY00503KA Specifications	
Resistance [k Ω]	50 ± 10 %
Rotation Angle [°]	300
Operating Temperature [°C]	-55 to 125
Shaft Diameter [mm]	6
Shaft Length [mm]	25

Table 3.11: Potentiometer specifications.



Figure 3.15: Potentiometer P11S1V0FLSY00503KA [14].

4. Levers

The levers act as a mechanical link between the spring or cables and the shafts. The longer the lever the less force needed by the springs to produce the maximum torque. The length of the lever can have several values, but, it has to be set to a length that allows reaching the maximum torque needed at the hinge, for the maximum spring elongation. A value of $s = 3 \text{ cm}$ has been chosen as an initial iteration, fig.3.16.

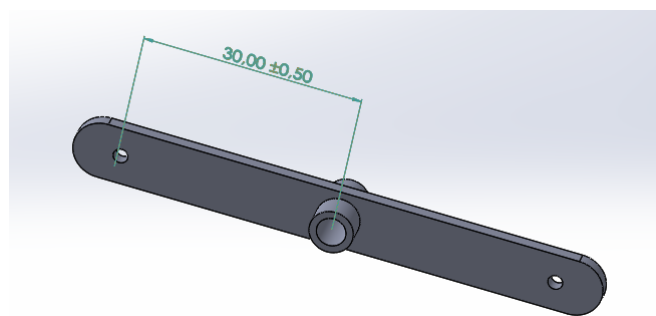


Figure 3.16: Lever, CAD.

5. Rods

Three rods are needed for this concept. One of the rods is driven by the servo motor (right rod), one is attached to a potentiometer and to the wing (inner left), and the other is attached to the potentiometer and has a free end (outer left), see fig3.2. The diameter and length of the rods are not critical values for the design. A diameter of $\phi = 4 \text{ mm}$ has been chosen, and the length will be adjusted as needed, fig.3.17.

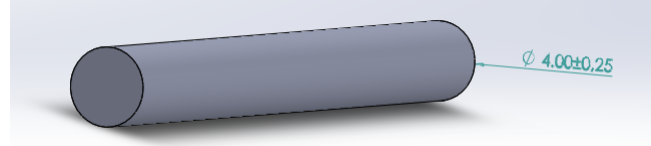


Figure 3.17: Rod, CAD.

6. Springs

The springs are the most critical component of this concept. To achieve a correct sizing, at the maximum spring elongation Δl_{max} , a torque of $\tau_{max}/2 \approx 2kg \cdot cm$ has to be reached. It is divided by 2 because the model will be built with half a wing.

Another aspect to consider is the pitch angle. According to REQ-2, the angle of attack α shall be between $\pm 20^\circ$. Assuming a horizontal air stream, it requires the pitch angle γ to be between $\pm 20^\circ$. The servo motor angle θ can be between 0 and 360 degrees, nonetheless, the range will be limited via software from 30 to 150 degrees. Therefore, the potentiometer angle ϕ will be between $\pm 40^\circ$ as $\phi = 90 - \theta_{min} - \gamma_{max} = 90 - 30 - 20 = 40$.

Combining equations eq.3.3, eq.3.4 and eq.3.5, eq3.8 is obtained.

$$\begin{aligned} \tau = 2s \cdot k(\sqrt{(l + s \cos \theta - s \cos(\theta + \phi))^2 + (s \sin \theta - s \sin(\theta + \phi))^2} - l) \cdot \\ \cos(90 - \phi - \theta - \arctan(\frac{s \sin(\theta + \phi) - s \sin \theta}{l + s \cos \theta - s \cos(\theta + \phi)})) \end{aligned} \quad (3.8)$$

A MatLab script has been written to obtain the value of τ for each combination of ϕ and θ , see appendix A.2.

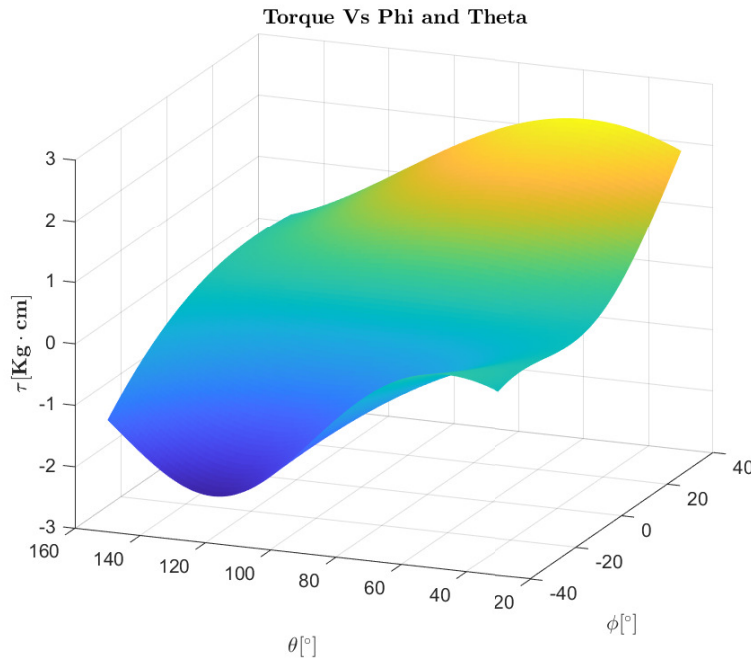


Figure 3.18: Torque values at the hinge for each phi and theta angle.

Plotting τ as in fig.3.18, a local maximum and minimum can be noticed. As mentioned before, in these points, τ should be at least $\tau = 2 \text{ Kg} \cdot \text{cm}$. With the next values, $k = 182 \text{ N/m}$, $l = 5.5 \text{ cm}$ and $s = 3 \text{ cm}$. Table 3.12 is obtained.

	$\tau [\text{kg} \cdot \text{cm}]$	$\phi [{}^\circ]$	$\theta [{}^\circ]$	$\Delta l [\text{mm}]$
Local maximum	2.2047	40	58	20.194
Local minimum	-2.308	-40	118	20.204

Table 3.12: Values of torque local maximum and minimum.

The spring that will be used is a tension spring, fig. 3.19, and it has the next characteristics.

Spring Specifications	
$k [\text{N/m}]$	182
$l_0 [\text{mm}]$	35
$\Delta l_{\max} [\text{mm}]$	47



Table 3.13: Tension spring specifications.

Figure 3.19: Tension spring [17].

The spring initial longitude is $l_0 = 35 \text{ mm}$, and as it can only perform in tension it is needed to be pre-tensed. As l was set to 5.5 cm the initial elongation will be 20 mm, and the maximum 75 mm.

7. Cables

Two cables will be used to link the outer left lever ends with the outer right lever. The length of the cables has to be equal to $l = 5.5 \text{ cm}$.

The cables only perform in tension, an important factor to take into account is its tensile strength at yield. Which for a **nylon 66** cable at 23°C is $\sigma_y = 84 \text{ MPa}$.

As the cables are attached to the outer left and right levers, they only receive force when the servo is in motion. And, this force will be always lower than $k \cdot \Delta l_{max} = 0.182 \text{ N/mm} \cdot 40 \text{ mm} \approx 7.3 \text{ N}$.

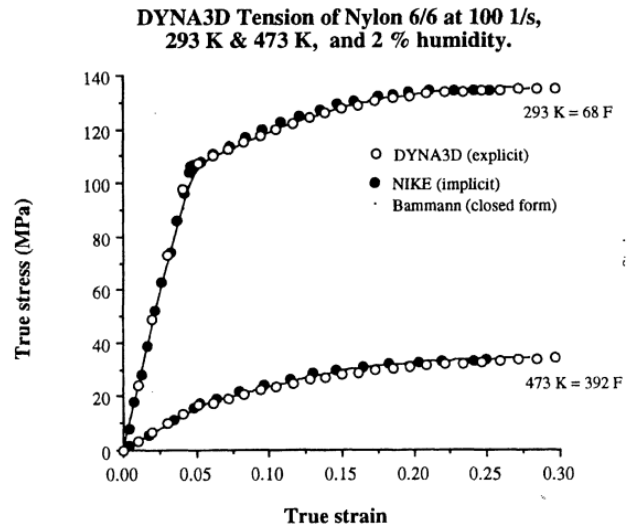


Figure 3.20: Stress over strain diagram for nylon 66. Extracted from p. 528 [22].

If a nylon 66 cable of $\phi = 1 \text{ mm}$ is used, the safety factor is:

$$S.F = \frac{84 \cdot 10^6}{7.3/10^{-3}} = 11.5 \cdot 10^3$$

8. Others

Other items may be needed to build the proof of concept, such as 3D printed pieces, screws, bearings, or glue, nevertheless, they are not critical components.

Concept 4

To build concept 4, next components are needed:

1. Gimbal motor

The gimbal motor will provide the torque directly to the hinge shaft. For the half wing, the maximum torque that can be given is $2 \text{ Kg}\cdot\text{cm}$. The proof of concept will be built with only half wing, so the load torque needed has to be at least $2 \text{ Kg}\cdot\text{cm}$.

The characteristics of the motor selected, fig.3.21, are the following:

iPower Motor GM5208-24	
Load Torque [Kg·cm]	1.8-2.5
Speed [rpm]	396 436
Weight [g]	207.8
Current [mA]	90
Configuration	24N22P

Table 3.14: iPower Motor GM5208-24 specifications.



Figure 3.21: Gimbal motor iPower Motor GM5208-24 [11].

2. BLDCM driver

The BLDCM driver will take the low-current signal from the Arduino Uno and amplify it into a high-current signal to correctly drive the motor. The driver chosen is the SimpleFOCShield v2.0.4, fig.3.22. This is an open-source low-cost motor driver board intended primarily for low-power FOC applications up to 5 Amps. The board is fully compatible with the Arduino UNO and all the boards with the standard Arduino headers. The SimpleFOCShield, in combination with the SimpleFOClibrary, provides a user-friendly way to control BLDC motors both in hardware and software.

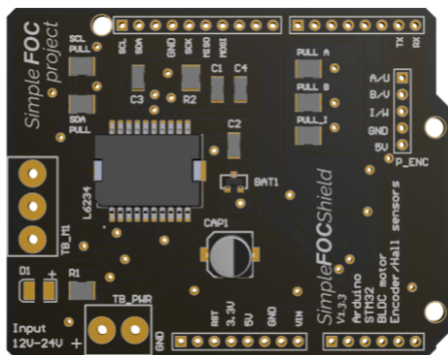


Figure 3.22: SimpleFOC board [10].

3. Micro-controller

The microcontroller that will be used for this concept is the same as concept 1. An Arduino UNO.

4. Motor encoder

The motor encoder is needed to measure the rotor angle θ . It has been chosen the magnetic sensor AS5X47U-TS-EK-AB, fig.3.23, it has the following features.

AS5X47U-TS-EK-AB	
Operating Supply Voltage [VDC]	3.3
Weight [g]	12.327

Table 3.15: AS5X47U-TS-EK-AB specifications.

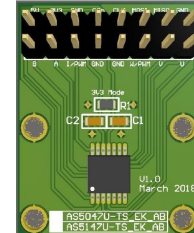


Figure 3.23: AS5X47U-TS-EK-AB magnetic encoder [12].

3.6.3 Final Design & Code

Concept 1

Finally, concept 1 will look as in fig.3.24. The cable connections have not been modeled due to simplicity reasons. The wiring diagram can be found ahead.

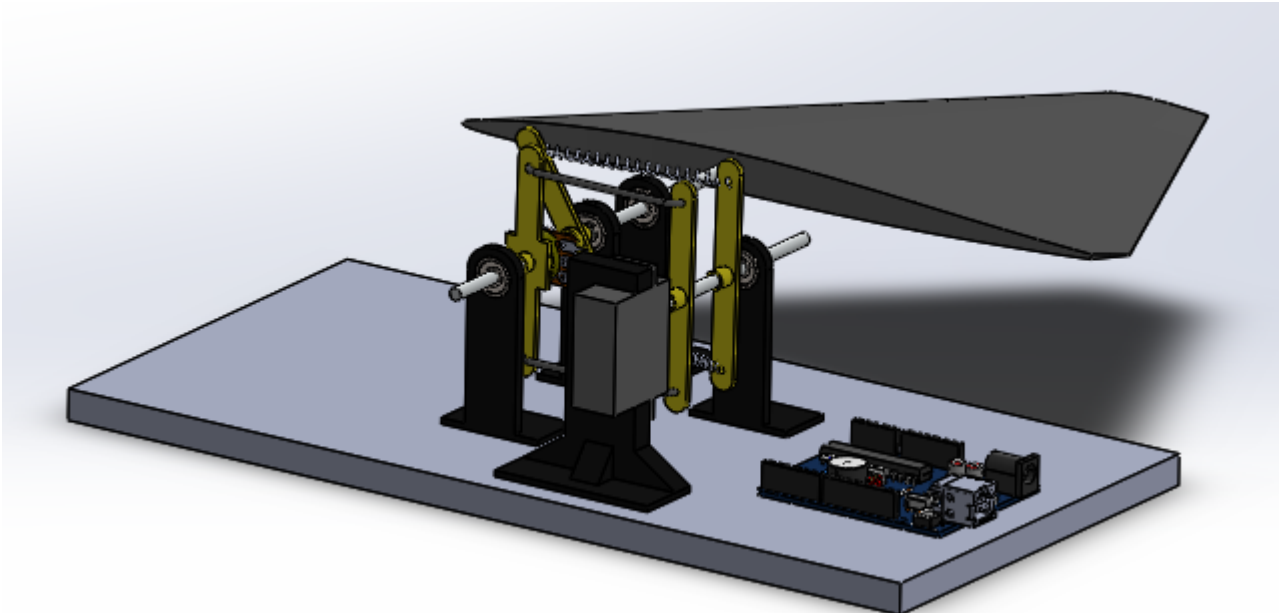


Figure 3.24: Concept 1, CAD.

To run concept 1, the following code has to be executed by the microcontroller.

First, the actuator pins, sensor pins, and some constants are defined. Also, the serial monitor is initialized.

```
#include<Servo.h>

Servo Servo1;

// Pins
int servoPin = 9;
int potPhi = A0;
int potAngle = A1;
int potForce = A2;

// Constants
int k = 182;
float l = 0.055;
float s = 0.03;
float pi = 3.14159265359;

void setup() {
  Servo1.attach(servoPin);
  Serial.begin(9600);
}
```

Afterwards, angles ϕ , θ , and β are calculated so the force produced by the wing can be known.

```
void loop() {

  float phi = (pi*map(analogRead(potPhi) - 511, -512, 511, -20, 20)) / 180.0;
  float theta = (pi*Servo1.read()) / 180.0;
  int setAngle = analogRead(potAngle);
  float setForce = 0.34 - (17*analogRead(potForce)) / 25575.0;

  float F = -k*(sqrt(pow(l+s*cos(theta)-s*sin(pi/2-theta-phi), 2)+pow(s*sin(theta)-s*cos(pi/2-theta-phi), 2))-1);
```

Once the force is known, the error between the desired force and the actual force is calculated. Therefore, the servomotor will rotate to reduce the error.

```
float error = setForce - F;

int angleS = map(setAngle, 0, 1023, 0, 180);
Servo1.write(angleS);

for (; (phi < 0 && error > 0); angleS -= 1){
  Servo1.write(angleS);
  delay(15);
```

```

phi = (pi*map(analogRead(potPhi) - 511,-512,511,-20,20))/180.0;
theta = (pi*Servo1.read())/180.0;
F = -k*(sqrt(pow(1+s*cos(theta)-s*sin(pi/2-theta-phi),2)+pow(s*sin(theta)-s*cos(pi/2-theta-phi),2))-1);
setForce= 0.34 - (17*analogRead(potForce))/25575.0;
error = setForce - F;
Serial.println(error);
}

Serial.println(error);
delay(1); // delay in between reads for stability
}

```

Finally, the error is calculated again entering a loop to always maintain it low. As it can be noticed the servo rotational speed is only proportional to the error. Integral and derivative constants have not been introduced due to simplicity reasons. Nevertheless, more tuning is needed to achieve better control performance. Full code in appendix A.3.

The wiring diagram of concept 1 is represented in fig.3.25. It is simple as only three electronic devices are used.

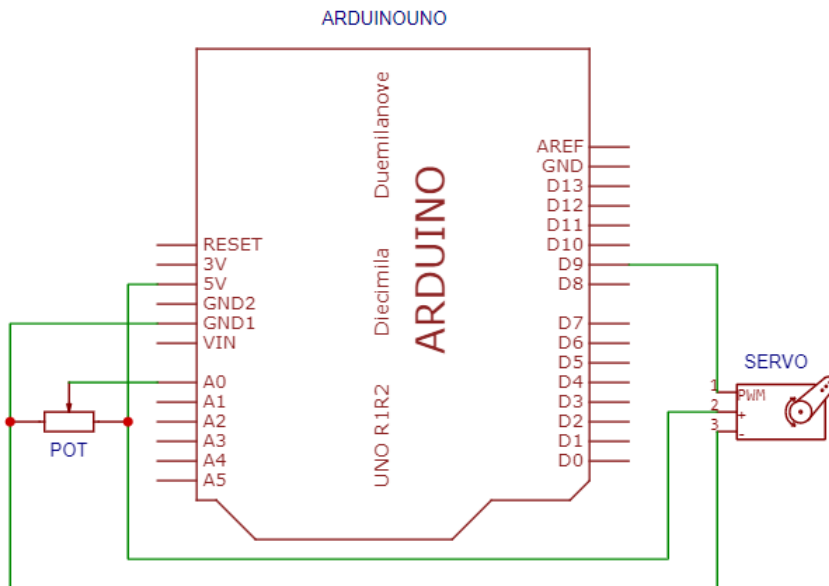


Figure 3.25: Concept 4, wiring diagram

The analog signal of the potentiometer is connected to A0 pin of the Arduino board. The PWM input of the servo motor is connected to the digital pin D9. Both the servo and potentiometer are connected in parallel to 5 V.

Concept 4

Concept 4 will look as in fig.3.26.

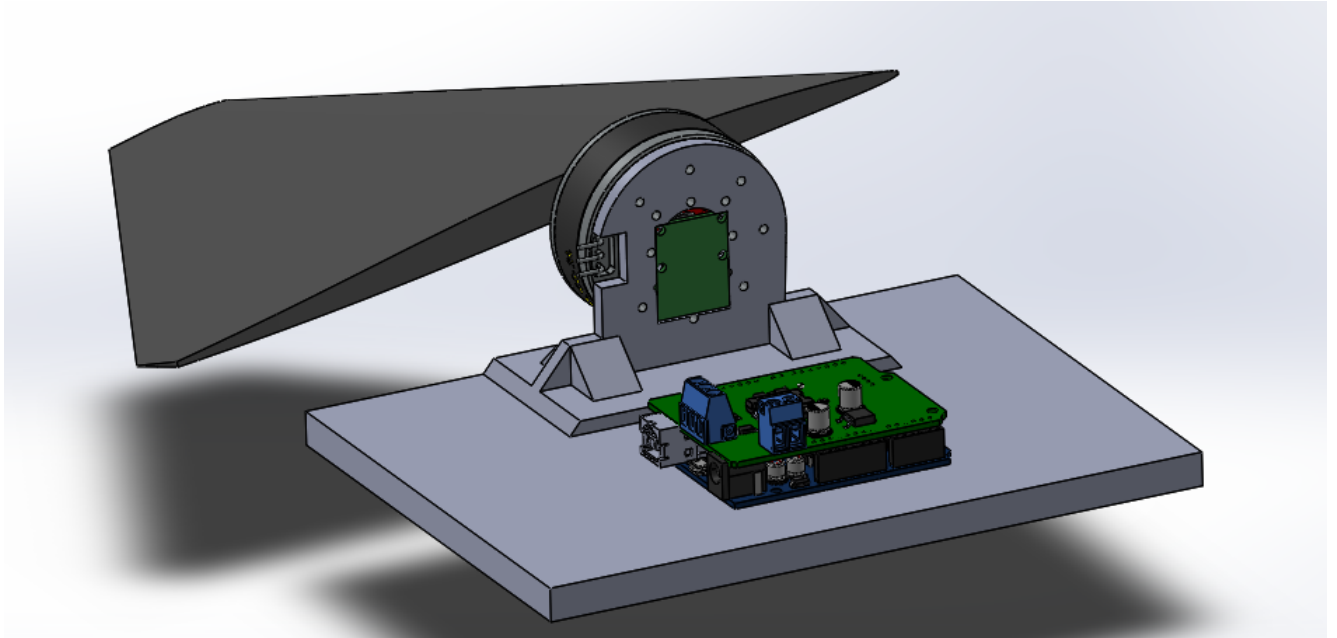


Figure 3.26: Concept 4, CAD.

As mentioned before, to control the torque within this concept, FOC will be used. An open-source library called Arduino SimpleFOClibrary [2] is used to implement FOC. The following code is extracted from the library and it is intended to do a torque control by adjusting the voltage of the BLDCM. Full code in appendix A.4.

First, it is needed to define the BLDCM class with the number of pole pairs (11) and the BLDC driver 3PWM class with the PWM pin numbers .

```
#include <SimpleFOC.h>

// BLDC motor & driver instance
BLDCMotor motor = BLDCMotor(11);
BLDCDriver3PWM driver = BLDCDriver3PWM(9, 5, 6, 8);
```

Afterwards, the magnetic encoder class is defined. It communicates with the board using an SPI protocol.

```
// magnetic sensor instance - SPI
MagneticSensorSPI sensor = MagneticSensorSPI(AS5147_SPI, 10);
```

Next, the voltage target is defined, and the desired voltage command is created.

```
// voltage set point variable
float target_voltage = 2;
// instantiate the commander
Commander command = Commander(Serial);
void doTarget(char* cmd) { command.scalar(&target_voltage, cmd); }
```

In the setup, the magnetic encoder and driver are connected to the motor, the hardware is initialized, the FOC algorithms are started and the power supply is set to 12 V.

Moreover, the FOC algorithms are set do a torque control loop.

```
void setup() {
    // initialise magnetic sensor hardware
    sensor.init();
    // link the motor to the sensor
    motor.linkSensor(&sensor);

    // power supply voltage
    driver.voltage_power_supply = 12;
    driver.init();
    motor.linkDriver(&driver);

    // aligning voltage
    motor.voltage_sensor_align = 5;
    // choose FOC modulation (optional)
    motor.foc_modulation = FOCModulationType::SpaceVectorPWM;
    // set motion control loop to be used
    motor.controller = MotionControlType::torque;

    // use monitoring with serial
    Serial.begin(115200);
    // comment out if not needed
    motor.useMonitoring(Serial);

    // initialize motor
    motor.init();
    // align sensor and start FOC
    motor.initFOC();

    // add target command T
    command.add('T', doTarget, "target voltage");

    Serial.println(F("Motor ready."));
    Serial.println(F("Set the target voltage using serial terminal:"));
    _delay(1000);
}
```

Finally, the motor is set in the FOC routine in the loop function. And the desired voltage is asked at the serial monitor.

```
void loop() {  
  
    // main FOC algorithm function  
    motor.loopFOC();  
  
    // Motion control function  
    motor.move();  
    if (Serial.available()) {  
        target_voltage = Serial.parseInt();  
    }  
  
    // user communication  
    command.run();  
}
```

The wiring diagram for concept 4, can be seen in fig.3.27.

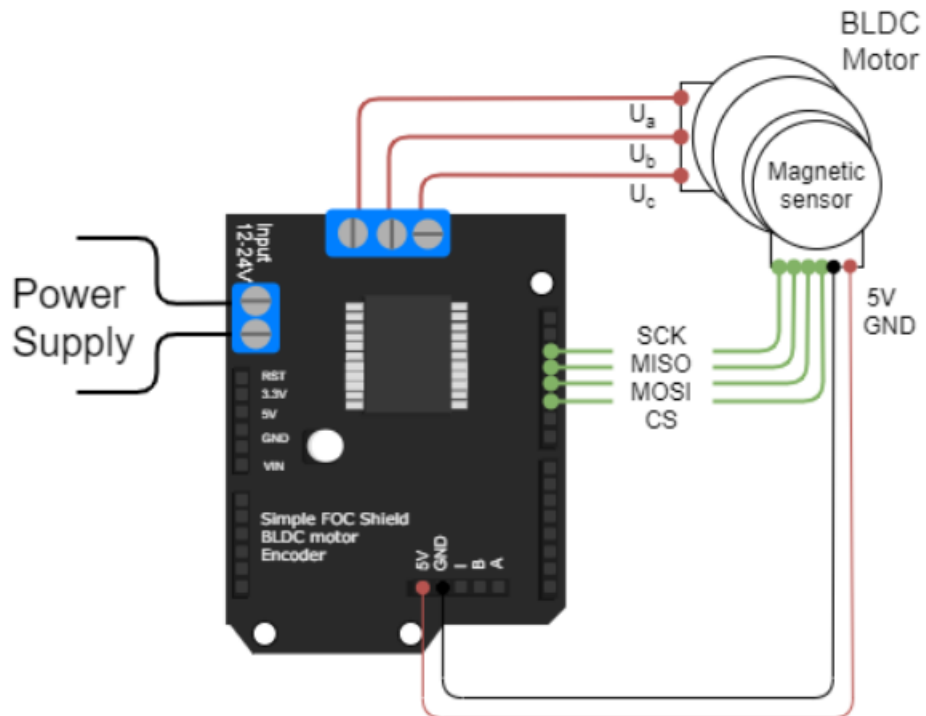


Figure 3.27: Concept 4, wiring diagram [Extracted from \[2\]](#).

Chapter 4

Analysis & Results

In this chapter, an analysis of the concepts is carried out. The natural oscillation frequency is studied, results of the build proofs of concepts are presented, improvements are proposed and the next logical steps for this project are discussed.

4.1 Resonance Frequency

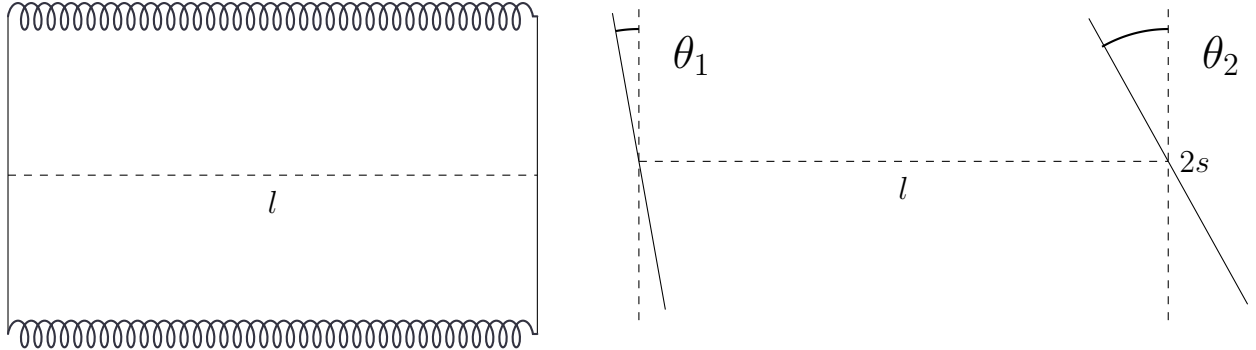
The resonant frequency of a mechanical system is understood as the characteristic frequency that reaches the maximum amplitude of oscillation caused by excitation from an external source. For a rotating mass, this amplification occurs at the critical speed. Every system has one or more characteristic frequencies. When a system is excited at one of its characteristic frequencies, its vibration is the maximum possible.

Electrical resonance causes an amplification of the magnitude of voltage or current, or both. The increase in amplitude, whether mechanical or electrical, increases the stress on motor components and negatively affects operation, e.g., increased vibration, instability, increased energy consumption, and premature failure.

By receiving energy from an external source, the resonant condition can cause the magnitude of the disturbance to continue to increase until a fault occurs. Mechanical resonance can lead to breakage of motor and drive components, and electrical resonance can result in winding failure.

4.1.1 Mechanical resonance frequency

To study the mechanical resonance frequency of concept 1 small angles of oscillation θ_1 and θ_2 are going to be assumed.



The force produced by the upper spring will be equal to:

$$F_u = k[s(\sin \theta_1 - \sin \theta_2) + l_0] \approx k[s(\theta_1 - \theta_2) + l_0]$$

And the force produced by the lower spring is:

$$F_d = -k[s(\sin \theta_1 - \sin \theta_2) - l_0] \approx -k[s(\theta_1 - \theta_2) - l_0]$$

Applying Newton's second law to the levers, the next coupled differential equations are obtained.

$$I_1 \ddot{\theta}_1 = -k[s(\theta_1 - \theta_2) + l_0]s - k[s(\theta_1 - \theta_2) - l_0]s$$

$$I_2 \ddot{\theta}_2 = k[s(\theta_1 - \theta_2) + l_0]s + k[s(\theta_1 - \theta_2) - l_0]s + \tau_0 \cos \omega t$$

Being,

$$I_1 = I_{Wing} + I_{InnerLeftLever} + I_{InnerLeftRod}$$

$$I_2 = 2I_{RightLever} + I_{OuterLeftLever} + I_{OuterLeftRod} + I_{RightRod}$$

The angles theta one and two can be expressed with a simple wave function.

$$\theta_1(t) = \Theta_1 \cos \omega t \quad \theta_2(t) = \Theta_2 \cos \omega t$$

By substituting the above equations,

$$-I_1 \Theta_1 \omega^2 = -k[s(\Theta_1 - \Theta_2) + l_0]s - k[s(\Theta_1 - \Theta_2) - l_0]s$$

$$-I_2 \Theta_2 \omega^2 = k[s(\Theta_1 - \Theta_2) + l_0]s + k[s(\Theta_1 - \Theta_2) - l_0]s + \tau_0 \cos \omega t$$

$$\begin{pmatrix} 2ks^2 - I_1 \omega^2 & -2ks^2 \\ -2ks^2 & 2ks^2 - I_2 \omega^2 \end{pmatrix} \begin{pmatrix} \Theta_1 \\ \Theta_2 \end{pmatrix} = \begin{pmatrix} 0 \\ \tau_0 \end{pmatrix}$$

Resonance will be achieved for the eigenvalues of the matrix determinant. That is to say,

$$I_1 I_2 \omega^4 - 2ks^2(I_1 + I_2)\omega^2 + 4k^2 s^4 - 4ks^4 = 0 \quad (4.1)$$

Whose solution is,

$$\omega_{1,2,3,4} = \pm \sqrt{\frac{2ks^2(I_1 + I_2) \pm \sqrt{(2ks^2(I_1 + I_2))^2 - 4I_1 I_2(4k^2 s^4 - 4ks^4)}}{2I_1 I_2}}$$

$$\omega_1 = +\sqrt{\frac{2ks^2(I_1 + I_2)}{I_1 I_2}}, \quad \omega_2 = -\sqrt{\frac{2ks^2(I_1 + I_2)}{I_1 I_2}}, \quad \omega_{3,4} = 0$$

Furthermore, applying the Crammer rule to find Θ_2 and searching ω to make the numerator equal to zero.

$$\Theta_2 = \frac{\begin{vmatrix} 2ks^2 - I_1 \omega^2 & 0 \\ -2ks^2 & \tau_0 \end{vmatrix}}{I_1 I_2 \omega^4 - 2ks^2(I_1 + I_2)\omega^2} = \frac{(2ks^2 - I_1 \omega^2)\tau_0}{I_1 I_2 \omega^4 - 2ks^2(I_1 + I_2)\omega^2} =$$

It is found that, at a frequency of

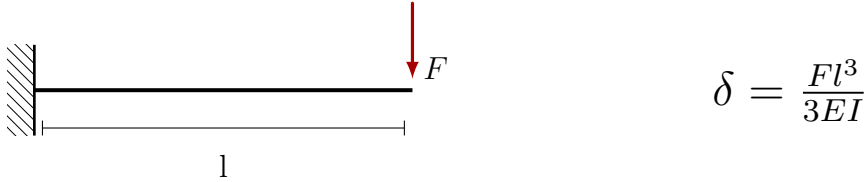
$$\omega = \sqrt{\frac{2ks^2}{I_1}}$$

the system will not oscillate.

Regarding concept 4, the canard wing is directly attached with a shaft to the gimbal motor. Unlike concept 1, there are no oscillating components in between the springs or levers. Therefore, the resonance will be purely electrical. Nevertheless, unbalances on the rotor or the shaft not being stiff enough, could cause mechanical vibrations.

It is known that the deflection in a cantilever δ follows the next expression. The maximum force produced by the wing will be:

$$F_{max} = mg \cos \alpha_{min} - L \cos \alpha_{min} - D \sin \alpha_{min}$$



Knowing the Young modulus of the shafts and their inertia, maximum deflection can be calculated.

4.1.2 Electrical resonance frequency

The power supplied to the servo motor in concept 1 is a PWM signal which duty-cycle can be changed to spin the motor clockwise or anti-clockwise. However, the rotational speed

remains constant and therefore the PWM frequency over time in a steady state phase.

On the other hand, in concept 4, the power is supplied with SPWM, meaning that the duty cycle constantly changes to reproduce a sine wave. The objective is to have pure sine waves at the fundamental frequency. Nevertheless, connecting non-linear loads to the power system can inject undesirable harmonic components. A variable frequency drive VFD as the simpleFOC usually produces undesirable harmonic components at the fifth or seventh harmonics. Harmonics increase losses in the power system and electrical equipment. Potentially the most detrimental effect of harmonics is that they could excite a system resonance that damages motors and even causes system failure.

For a gimbal motor, the electrical resonance frequency can be calculated with eq. 4.2

$$f = \frac{100}{2\pi} \sqrt{\frac{2n_{pp}M_h}{J_r}} \quad (4.2)$$

Where, M_h is the holding torque in Nm , n_{pp} is the number of pole pairs, and J_r is the rotor inertia in $kg \cdot m^2$.

It is worth mentioning that it has been presented the formula to calculate the resonance frequencies and deflection of the concepts. But, the numerical results have not been calculated. To obtain these results, the inertia of the canard wing has to be known, as it is 3D printed with an interior reinforcement pattern the density is not equal among the wing. Therefore calculating the inertia would require a certain amount of time, as the 3D printing software does not provide the result. Furthermore, the aim of the proofs of concepts it is just to prove that functioning principles can work. Thus obtaining the numerical results has not been considered worth it in this scenario.

4.2 Models performance

Once both concepts have been built, the results obtained match the expectations of the project. During the manufacturing process, some changes have been applied to the design of the concepts to improve their performance.

For **concept 1**, instead of using a potentiometer to measure the angle difference between levers, a magnetic sensor has been used and fed back directly to the servo motor. This way, no external microcontroller is needed and the own servo motor calculates the torque to be produced, this torque can be controlled with a PWM signal. However, the initial design is not wrong and an external microcontroller can be used to implement different control strategies and overcome disturbances and faults in different ways. Moreover, cables to link the outer levers have not been used, in their place a push-pull rod has been used.

The next figure, fig.4.1, shows the first concept built.

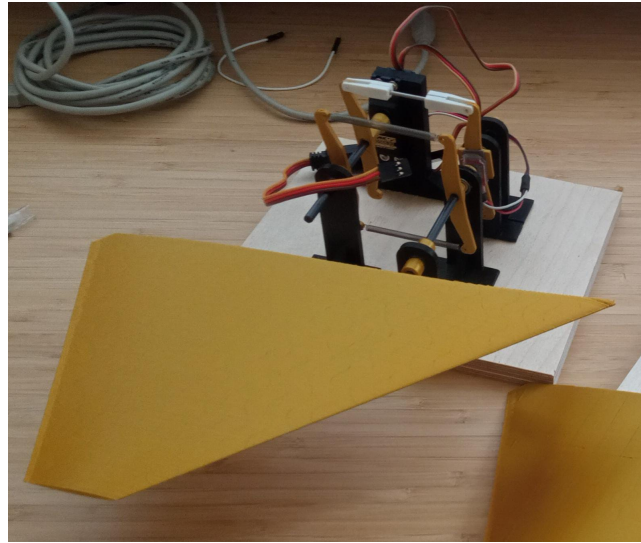


Figure 4.1: Concept 1, real model.

The behavior of the mock-up is not perfectly linear, it presents slight oscillations and the servo motor is quite loud. When the servo motor operates at maximum force without any opposition the springs make contact with the levers.

Concept 4 has maintained its initial design. The motor rotates smoothly producing a constant torque without cogging. This concept is more robust and silent than the previous but it requires much more power to operate and it is considerably heavier.

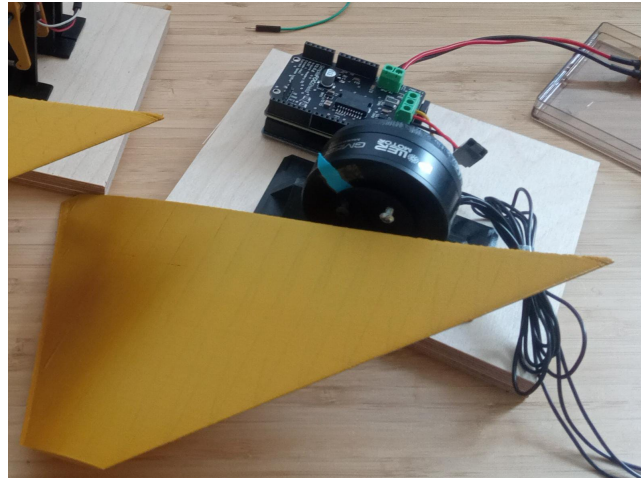


Figure 4.2: Concept 4, real model.

It has been noticed a motor resistance at 0 V which could be problematic when the wing is required to align with the free stream. This is because initially, the only parameter specified to the simpleFOC library was the number of pole pairs. Therefore, the current estimation that is done and given to each phase is not accurate enough. This problem can be solved by specifying the motor's internal resistance and velocity rating so the library can automatically calculate the appropriate voltage while compensating for the generated

back EMF. The phase inductance can be also specified to compensate for the lag of the torque vector by calculating an appropriate d-axis voltage.

```
#include <SimpleFOC.h>

// BLDCMotor(pole pairs, internal resistance [ohms], kv rating [rpm/V],
// phase inductance [H])
BLDCMotor motor = BLDCMotor( 11, 1, 35, 0.001 );
```

These parameters can be adjusted in different ways to achieve the desired performance. The higher the specified internal resistance, the lower voltage is needed to produce torque as the intensity raises. The higher the kv rating the lower is the back EMF estimation, the back EMF is defined as $U_{bemf} = k_{bemf} \cdot v = \frac{1}{kv} \cdot v$, even though, in reality, the back EMF constant will be always lower than the inverse of the velocity rating $k_{bemf} < \frac{1}{kv}$, it is still a good approximation.

By raising the inductance value L , motor velocity will increase until reaching a certain value where it will start to decrease. The optimum L value is the minimum one that achieves maximum velocity.

Thus, the direct and quadrature components of the voltage, U_d , U_q follow the next expressions.

$$U_d = -I_d L v n_{pp} \quad (4.3)$$

$$U_q = IR + \frac{v}{kv} \quad (4.4)$$

The parameters shown above, $n_{pp} = 11$, $R = 1 \Omega$, $kv = 35 \text{ rpm/V}$, $L = 0.001 \text{ H}$. Have shown experimentally low motor resistance at 0 V, smooth motion, and appropriate velocity and torque.

Lastly, in appendix A.5 a program able to change from position to force control has been written.

4.3 Improvements

After analyzing the performance of both concepts, the following improvements are proposed for the next iterations.

Regarding **concept 1**.

It can be noticed that the mechanism occupies a significant amount of volume. One way to reduce it would be using shorter lever arms. This modification would lead to using stiffer springs with a higher spring constant to maintain the same amount of torque produced at the shafts. However, it has to be taken into account that the mechanical resonance frequency of the new springs, studied in section 4.1.1, is not reached.

Changing initial parameters s and k of the program written to size the springs in 6 to $s = 6 \text{ mm}$ and $k = 5000 \text{ N/m}$ keeps a torque of $\tau = 2.4 \text{ kg} \cdot \text{cm}$ at the Hinge. The size of this new spring compared to the initial one can be seen in fig.4.3.

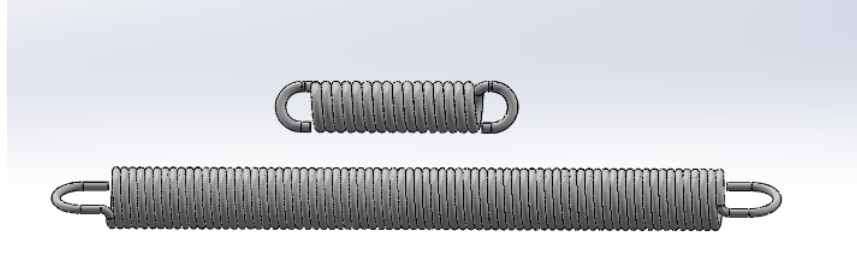


Figure 4.3: Size comparison between springs.

This alternative spring would allow a considerable decrease in the volume of the force-sensing mechanism. Different combinations of s and k can be tested until achieving the most suitable for a particular aircraft. It is worth mentioning that, whenever a change is introduced, analysis is needed to ensure compatibility between components and requirements.

Regarding **concept 4**.

The main drawback of concept 4 is its weight and power consumption. The motor used for the proof of concept is slightly oversized. Nevertheless, a better-sized actuator would also be heavier than the servo motor of concept one. To decrease the weight of the motor the use of a gearbox could be studied to increase the torque of a smaller BLDCM.

Furthermore, the sensor used to determine the rotor's position is a magnetic sensor, it is a suitable and affordable option. However, it is believed that an encoder would be a better option as it can be more precise, there is less noise and is not easily influenced by magnetic fields that could be produced by other components of the aircraft.

4.4 Next steps

The objective of this thesis has been successfully achieved. The next logical steps for this project are going to be discussed in this section.

1. The first step would be to implement the improvements proposed in section 4.3. The occupied volume of concept 1 and the weight of concept 4 should be minimized until reaching an optimum value.
2. Next, the control parameters should be tuned according to the requirements set by the customers and the type of aircraft. A robust system capable of overcoming disturbances is desirable.

3. Once the concepts are optimized, and the control parameters are tuned. The systems need to be tested in conditions close to real flight conditions to validate their functioning.
4. Finally, the last step would be to implement the mechanisms in a real UAV and carry out enough iterations of the systems until reaching the desired performance.

Conclusion

This project aimed to design a prototype system capable of delivering and controlling directly the force given to a canard wing. Four proofs of concept have been proposed and two of them have been successfully built. Nevertheless, not all of the initial requirements have been met by both concepts.

Requirements REQ-1 and REQ-2 established some of the flight conditions, a maximum cruise speed of 150 km/h , and an angle of attack range of $\pm 20^\circ$. Knowing the wing's geometry, an aerodynamic analysis has been carried out in order to size the actuators to handle the forces produced by the wing in such conditions. The material used to build the two selected proofs of concept was mainly 3D printed pieces and actuators and sensors available at the FLUMES department. The proofs of concepts are oversized and can handle more torque than the produced by the half wing. Hence, the first two requirements should be fulfilled. Nonetheless, further testing, such as using a wind tunnel or using the mechanism in a real UAV may be carried out to validate the first two requirements.

Regarding REQ-3, on one hand, concept 1 can be considered lightweight, being the servomotor the heaviest piece of the mechanism with a mass of 28 g. On the other hand, the heaviest component of concept 4 is the BLDCM with a mass of 204 g which is significantly more than the former. Moreover, concept 1 meets REQ-4 achieving a torque of $4 \text{ kg} \cdot \text{cm}$ with a voltage supply of 6 V, concept 4, does not meet the requirement as it needs 20 V to produce a load torque of $2.5 \text{ kg} \cdot \text{cm}$. Unlike the servomotor, the BLDCM does not make use of gears to increase torque.

That being said, the first concept may seem superior to the fourth as it meets all the initial requirements. However, concept 4 is more versatile, it would allow to change from position control to force control, it has fewer moving parts and occupies less volume.

Both concepts are considered suitable to be implemented in a UAV, to select which one is the best option for a particular kind of aircraft, more requirements are needed. Nevertheless, implementing the improvements mentioned in section 4.3 and considering the initial requirements set for this project, concept 1 seems to be the best option.

Bibliography

- [1] Advanced motion controls. Available in: <https://www.a-m-c.com/es/servo-drive-basics/>.
- [2] Simplefoc project. Available in: <https://docs.simplefoc.com/>.
- [3] Motor speed controller tutorial - pwm how to build. Available in: <https://www.youtube.com/watch?v=UPTU6nYSaMo&t=23s>.
- [4] Field-oriented control (vector control) for brushless dc motors. Available in: <https://control.com/technical-articles/field-oriented-control-vector-control-for-brushless-dc-motors/>.
- [5] Incremental encoder. Available in: https://en.wikipedia.org/wiki/Incremental_encoder.
- [6] Wheatstone bridge with gauges. Available in: https://commons.wikimedia.org/wiki/File:Wheatstone_bridge_with_gauges.jpg.
- [7] How servo motors work & how to control servos using arduino. Available in: <https://www.youtube.com/watch?v=LXURLvga8bQ>.
- [8] xf1r5. Available in: <http://www.xf1r5.tech/xf1r5.htm>.
- [9] Arduino uno. Available in: <https://store.arduino.cc/products/arduino-uno-rev3>.
- [10] Simplefocshield v2. Available in: <https://simplefoc.com/shop>.
- [11] Gimbal motor gm5208-24. Available in: <https://shop.iflight-rc.com/ipower-motor-gm5208-24-brushless-gimbal-motor-pro1347>.
- [12] Magnetic encoder. Available in: https://www.mouser.se/ProductDetail/ams-OSRAM/AS5X47U-TS_EK_AB?qs=u16ybLDytRbyyVYcz3f5gw%3D%3D.
- [13] Gimbal servo 360 mksds6630. Available in: <https://mks-servo.com/DS6630>.
- [14] P11s1v0flsy00503ka. Available in: <https://se.farnell.com/vishay/p11s1v0flsy00503ka/potentiometer-linj-r-50kohm-1w/dp/1141601>, .
- [15] Electronics basics – how a potentiometer works. Available in: <https://randomnerdtutorials.com/electronics-basics-how-a-potentiometer-works/>, .

- [16] Torque control using foc currents. Available in: https://docs.simplefoc.com/foc_current_torque_mode.
- [17] Spring 3677: Ess 0,4x3x35. Available in: <https://catalog.lesjoforsab.com/product/3677-ess-0-4x3x35>.
- [18] R. COLLINSON. *Introduction to Avionics Systems*. Springer, 2011.
- [19] U. S. department of transportation FEDERAL AVIATION ADMINISTRATION. *Pilot's Handbook of Aeronautical Knowledge*. Flight Standards Service, 2008.
- [20] E. A. Erlbacher. Force control basics. *PushCorp, Inc.*, 2000.
- [21] G. Q. et al. A review of electromechanical actuators for more/all electric aircraft systems. *Sage Journals*, 232, 2018. doi: <https://doi.org/10.1177/0954406217749869>.
- [22] G. A. Gazonas. Mimplementation of a finite strain plasticity model for nylon 6/6 into dyna3d. *U.S. Army Research Laboratory, Weapons and Materials Research*, 2000.
- [23] O. Gomis-Bellmunt and L. F. Campanile. *Design Rules for Actuators in Active Mechanical Systems*. Springer, 2010.
- [24] T. Instruments. Field-oriented control. Available in: https://www.youtube.com/watch?v=_6-_jvZe7iA&t=231s&ab_channel=TexasInstruments.
- [25] R. Kowalski, J. Windelberg, R. Ladner, and M. Rottach. Force fight compensation for redundant electro-mechanical flight control actuators. *International Council of the Aeronautical Sciences*, 2018. URL https://www.icas.org/ICAS_ARCHIVE/ICAS2018/data/papers/ICAS2018_0271_paper.pdf.
- [26] R. W. Pratt. *FLIGHT CONTROL SYSTEMS practical issues in design and implementation*. The Institution of Electrical Engineers, 2000.
- [27] D. P. Raymer. *Aircraft Design: A Conceptual Approach*. AIAA.
- [28] U. S. A. F. stability and control DATCOM. *Experimental low speed airfoil section aerodynamic characteristics*. USAF.
- [29] X. Sun, X. Wang, and S. Lin. Multi-fault diagnosis approach based on updated interacting multiple model for aviation hydraulic actuator. *Information*, 2020. doi: <https://doi.org/10.3390/info11090410>.
- [30] M. J. SUTHERLAND. Fly-by-wire flight control systems. *Joint Meeting of Flight Mechanics and Guidance and Control Panels of AGARD*, 1968.
- [31] Y. Yan, J. Ynag, C. Liu, M. Coombes, S. Li, and W.-H. Chaen. On the actuator dynamics of dynamic control allocation for a small fixed-wing uav with direct lift control. *IEEE*, 28, 2020. doi: 10.1109/TCST.2019.2945909.
- [32] K. Yokota and H. Fujimoto. Aerodynamic force control for tilt-wing evtol using airflow vector estimation. *IEEE*, 8, 2022. doi: 10.1109/TTE.2022.3162946.

- [33] A. Zaitsevsky. Force servo. [visited: 10 february 2023]. url: <http://myresearch.company/f-servo.phtml>.

Appendix A

Codes

A.1 Actuator sizing

Code used in section 2.2.2 to calculate the local maximum and minimum torque produced by the wing at the flight conditions set by the requirements.

```
1 clc
2 clear
3 close all

5 % Plotting Hinge moment vs Alpha
6 rho = 1.225; % Kg/m^3
7 U_inf = 42; % m/s
8 S = 0.032; % m^2
9 x_ac = 0.0383; % m
10 x_h = 0.0283; % m
11 x_cg = 0.08; % m 0.0765
12 CL_alpha = 0.0424; % 1/
13 CD0 = 0.0061;
14 CDi = 0.165;
15 m = 0.200; % kg
16 g = 9.81; % m/s

17 i=0;
18 for alpha=-20:0.05:20
19     i = i + 1;
20     tau(i) = 0.5*rho*U_inf^2*S*(x_ac-x_h)*(CL_alpha*alpha*cosd(alpha)+(CD0+
21         CDi*CL_alpha^2*alpha^2)*sind(alpha))-m*g*cosd(alpha)*(x_cg-x_h);
22 end
23 alpha = [-20:0.05:20];

25 plot(alpha,tau);
26 title(''$\mathbf{\tau}$ vs $\mathbf{\alpha}$'', 'interpreter', 'latex');
27 xlabel(''$\mathbf{\alpha}$ [ $^\circ$]', 'interpreter', 'latex');
28 ylabel(''$\mathbf{\tau}$ [ N$\cdot$cm ]'', 'interpreter', 'latex');
29 % xlim([-90 90])

31 t_max = max(abs(tau))
32 t = (t_max/g)*100/2 % kg*cm
```

A.2 Spring sizing

Code used in 6 to calculate the torque at the hinge for each combination of ϕ and θ .

```

2 s = 0.03; %m
k = 182; %N/m
4 l = 0.055; %m

6 j = 0;
i = 0;
8
10 theta_max = 0;
phi_max = 0;
tau_max = 0;
12 delta_l_max = 0;

14 theta_min = 0;
phi_min = 0;
16 tau_min = 0;
delta_l_min = 0;
18
20 for theta=30:1:150
j = j + 1;
22 for phi=-40:1:40
i = i + 1;
24 tau(j,i) = 2*s*k*((1+s*cosd(theta)-s*cosd(theta+phi))^2 + (s*sind(theta)-s*sind(theta+phi))^2)^0.5 - 1)*cosd(90-theta-phi-atand((s*sind(theta+phi)-s*sind(theta))/(1+s*cosd(theta)-s*cosd(theta+phi))));
if tau(j,i)>tau_max
26 tau_max = tau(j,i);
theta_max = theta;
phi_max = phi;
28
30 delta_l_max = ((1+s*cosd(theta)-s*cosd(theta+phi))^2 + (s*sind(theta)-s*sind(theta+phi))^2)^0.5 - 1;
end

32 if tau(j,i)<tau_min
34 tau_min = tau(j,i);
theta_min = theta;
phi_min = phi;
36 delta_l_min = ((1+s*cosd(theta)-s*cosd(theta+phi))^2 + (s*sind(theta)-s*sind(theta+phi))^2)^0.5 - 1;
end
38 end
i = 0;
40 end

```

A.3 Concept 1 full code

Code used in section 3.6.3 to control concept 1.

```
#include<Servo.h>

Servo Servo1;

// Pins
int servoPin = 9;
int potPhi = A0;
int potAngle = A1;
int potForce = A2;

// Constants
int k = 182;
float l = 0.055;
float s = 0.03;
float pi = 3.14159265359;

void setup() {
    Servo1.attach(servoPin);
    Serial.begin(9600);
}

void loop() {
    float phi = (pi*map(analogRead(potPhi) - 511, -512, 511, -20, 20)) / 180.0;
    float theta = (pi*Servo1.read()) / 180.0;
    int setAngle = analogRead(potAngle);
    float setForce = 0.34 - (17*analogRead(potForce)) / 25575.0;

    float F = -k*(sqrt(pow(l+s*cos(theta)-s*sin(pi/2-theta-phi), 2)+pow(s*sin(theta)-s*cos(pi/2-theta-phi), 2))-1);

    float error = setForce - F;

    int angleS = map(setAngle, 0, 1023, 0, 180);
    Servo1.write(angleS);

    for (; (phi<0 && error>0); angleS -=1){
        Servo1.write(angleS);
        delay(15);

        phi = (pi*map(analogRead(potPhi) - 511, -512, 511, -20, 20)) / 180.0;
        theta = (pi*Servo1.read()) / 180.0;
        F = -k*(sqrt(pow(l+s*cos(theta)-s*sin(pi/2-theta-phi), 2)+pow(s*sin(theta)-s*cos(pi/2-theta-phi), 2))-1);
        setForce = 0.34 - (17*analogRead(potForce)) / 25575.0;
        error = setForce - F;
        Serial.println(error);
    }
    delay(10); // delay in between reads for stability
}
```

A.4 Concept 4 full code

Code used in section 3.6.3 to control concept 4. Extracted from [2].

```
/*
 * Torque control example using voltage control loop.
 *
 * Most of the low-end BLDC driver boards doesn't have current measurement
 * therefore SimpleFOC offers
 * you a way to control motor torque by setting the voltage to the motor
 * instead hte current.
 *
 * This makes the BLDC motor effectively a DC motor, and you can use it in
 * a same way.
 */
#include <SimpleFOC.h>

// magnetic sensor instance - SPI
MagneticSensorSPI sensor = MagneticSensorSPI(AS5147_SPI, 10);
// magnetic sensor instance - I2C
// MagneticSensorI2C sensor = MagneticSensorI2C(AS5600_I2C);
// magnetic sensor instance - analog output
// MagneticSensorAnalog sensor = MagneticSensorAnalog(A1, 14, 1020);

// BLDC motor & driver instance
BLDCMotor motor = BLDCMotor(11);
BLDCDriver3PWM driver = BLDCDriver3PWM(9, 5, 6, 8);
// Stepper motor & driver instance
//StepperMotor motor = StepperMotor(50);
//StepperDriver4PWM driver = StepperDriver4PWM(9, 5, 10, 6, 8);

// voltage set point variable
float target_voltage = 2;
// instantiate the commander
Commander command = Commander(Serial);
void doTarget(char* cmd) { command.scalar(&target_voltage, cmd); }

void setup() {

    // initialise magnetic sensor hardware
    sensor.init();
    // link the motor to the sensor
    motor.linkSensor(&sensor);

    // power supply voltage
    driver.voltage_power_supply = 12;
    driver.init();
    motor.linkDriver(&driver);

    // aligning voltage
    motor.voltage_sensor_align = 5;
    // choose FOC modulation (optional)
    motor.foc_modulation = FOCModulationType::SpaceVectorPWM;
    // set motion control loop to be used
    motor.controller = MotionControlType::torque;
```

```
// use monitoring with serial
Serial.begin(115200);
// comment out if not needed
motor.useMonitoring(Serial);

// initialize motor
motor.init();
// align sensor and start FOC
motor.initFOC();

// add target command T
command.add('T', doTarget, "target voltage");

Serial.println(F("Motor ready."));
Serial.println(F("Set the target voltage using serial terminal:"));
_delay(1000);
}

void loop() {

// main FOC algorithm function
// the faster you run this function the better
// Arduino UNO loop ~1kHz
// Bluepill loop ~10kHz
motor.loopFOC();

// Motion control function
// velocity, position or voltage (defined in motor.controller)
// this function can be run at much lower frequency than loopFOC()
// function
// You can also use motor.move() and set the motor.target in the code
motor.move(target_voltage);
if (Serial.available()){
    target_voltage = Serial.parseInt();
}

// user communication
command.run();
}
```

A.5 Concept 4 Position & Force Control

Program to change from position control to force control, being the position and force set by a PWM signal via a radio controller.

```
#include <SimpleFOC.h>

const int numReadings = 16; // Number of readings for moving average
const int threshold = 35; // Hysteresis threshold
int readings[numReadings]; // Array to store the readings
int index = 0; // Index of the current reading
int total = 0; // Total sum of readings
volatile int sensorValue = 0; // Global variable for the sensor value

const int minAngle = -20; // Minimum angle in degrees
const int maxAngle = 20; // Maximum angle in degrees

const int minVoltage = -6; // Minimum angle in Volts
const int maxVoltage = 6; // Maximum angle in Volts

float angle_offset = 0;
float n = 0;

// magnetic sensor instance - SPI
MagneticSensorSPI sensor = MagneticSensorSPI(AS5147_SPI, 10);
// rc signal - PWM - MagneticSensorPWM(PIN, m_raw_count, max_raw_count)
MagneticSensorPWM rc_signal = MagneticSensorPWM(2, 960, 1984);
void doPWM(){rc_signal.handlePWM();}

// BLDC motor & driver instance
//BLDCMotor motor = BLDCMotor(11, 1, 35, 0.001);
BLDCMotor motor = BLDCMotor(11);
BLDCDriver3PWM driver = BLDCDriver3PWM(9, 5, 6, 8);

// control type
bool Force_control = false;

// voltage set point variable
float target_voltage = 1;
float target_voltage_next = 0;
// angle set point variable
float target_angle = 0;
int target_angle_next = 0;

// instantiate the commander
Commander command = Commander(Serial);
void doTargetA(char* cmd) {
    command.scalar(&target_voltage, cmd);
}
void doTargetB(char* cmd) {
```

```
    command.scalar(&target_angle, cmd);  
}  
void controlType(char* cmd) {  
    if (cmd[0] == '0') Force_control = false;  
    else if (cmd[0] == '1') Force_control = true;  
}  
  
void setup() {  
  
    // initialise magnetic sensor hardware & rc receiver  
    sensor.init();  
    rc_signal.init();  
  
    // allow rc signal interruptions  
    rc_signal.enableInterrupt(d0PWM);  
  
    for (int i = 0; i < numReadings; i++) {  
        readings[i] = 0;  
    }  
  
    // link the motor to the sensor  
    motor.linkSensor(&sensor);  
  
    // power supply voltage [V]  
    driver.voltage_power_supply = 12;  
    driver.init();  
    motor.linkDriver(&driver);  
  
    // aligning voltage  
    motor.voltage_sensor_align = 5;  
    // choose FOC modulation (optional)  
    motor.foc_modulation = FOCModulationType::SpaceVectorPWM;  
  
    if (Force_control) {  
        motor.controller = MotionControlType::torque;  
    } else {  
        motor.controller = MotionControlType::angle;  
    }  
  
    // controller configuration  
    // default parameters in defaults.h  
  
    // velocity PI controller parameters  
    motor.PID_velocity.P = 0.5f;  
    motor.PID_velocity.I = 30;  
    motor.PID_velocity.D = 0.;  
    // maximal voltage to be set to the motor  
    motor.voltage_limit = 10;  
  
    // velocity low pass filtering time constant  
    // the lower the less filtered  
    motor.LPF_velocity.Tf = 0.01f;  
  
    // angle P controller  
    motor.P_angle.P = 20;  
    // maximal velocity of the position control
```

```
    motor.velocity_limit = 20;
}

// use monitoring with serial
Serial.begin(115200);

// comment out if not needed
motor.useMonitoring(Serial);
// initialize motor
motor.init();
// align sensor and start FOC
motor.initFOC();

// add target command
command.add('V', doTargetA, "target voltage");
command.add('A', doTargetB, "target angle");
command.add('C', controlType, "control type");

Serial.println(F("Commander listening"));
Serial.println(F(" — Send C0 to position control"));
Serial.println(F(" — Send C1 to force control"));

Serial.println(F("Motor ready."));
if (Force_control) {
    Serial.println(F("Set the target voltage using the command V:"));
} else {
    Serial.println(F("Set the target angle using command A:"));
}
_delay(1000);
}

void loop() {
motor.loopFOC();

sensorValue = rc_signal.pulse_length_us;

// Subtract the oldest reading from the total
total -= readings[index];
// Store the new reading in the array and add it to the total
readings[index] = sensorValue;
total += readings[index];
// Move to the next index
index++;
if (index >= numReadings) {
    index = 0;
}
// Calculate the average
int average = total / numReadings;

// Apply hysteresis
static int outputValue = 0; // Holds the filtered output value

if (abs(average - outputValue) > threshold) {
```

```
    outputValue = average;
}

if (Force_control) {
    forceControl(outputValue);
} else {
    positionControl(outputValue);
}

// user communication
command.run();
}

void forceControl(int average) {
motor.controller = MotionControlType::torque;
motor.move(target_voltage);
target_voltage = map(average, 960, 1984, minVoltage, maxVoltage);

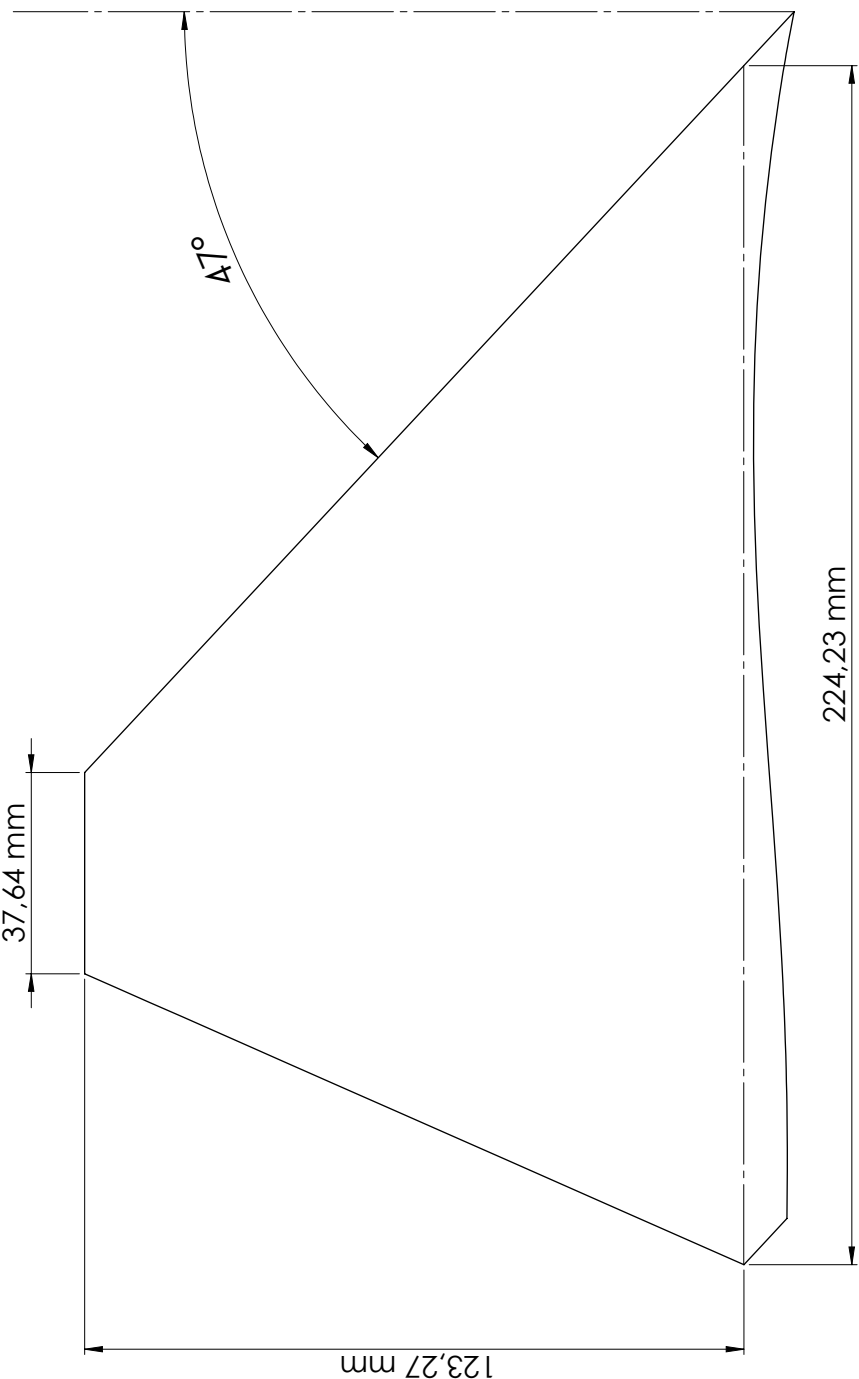
n = abs(sensor.getAngle()) / 6.28;
if ((2 * int(n) + 1) > n and n < 2 * int(n)) {
    angle_offset = (sensor.getAngle() - (n - int(n)) * 6.28);
} else {
    angle_offset = (sensor.getAngle() + ((1 - n - int(n)) * 6.28));
}

Serial.print("Voltage: ");
Serial.println(target_voltage);
}

void positionControl(int average) {
motor.controller = MotionControlType::angle;
motor.sensor_offset = angle_offset;
motor.move(target_angle * (3.14159265359 / 180.0)); // move motor in
radians
target_angle = map(average, 960, 1984, minAngle, maxAngle); // set the
target angle via PWM signal and convert it to degrees
Serial.print("Angle: ");
Serial.println(target_angle);
}
```

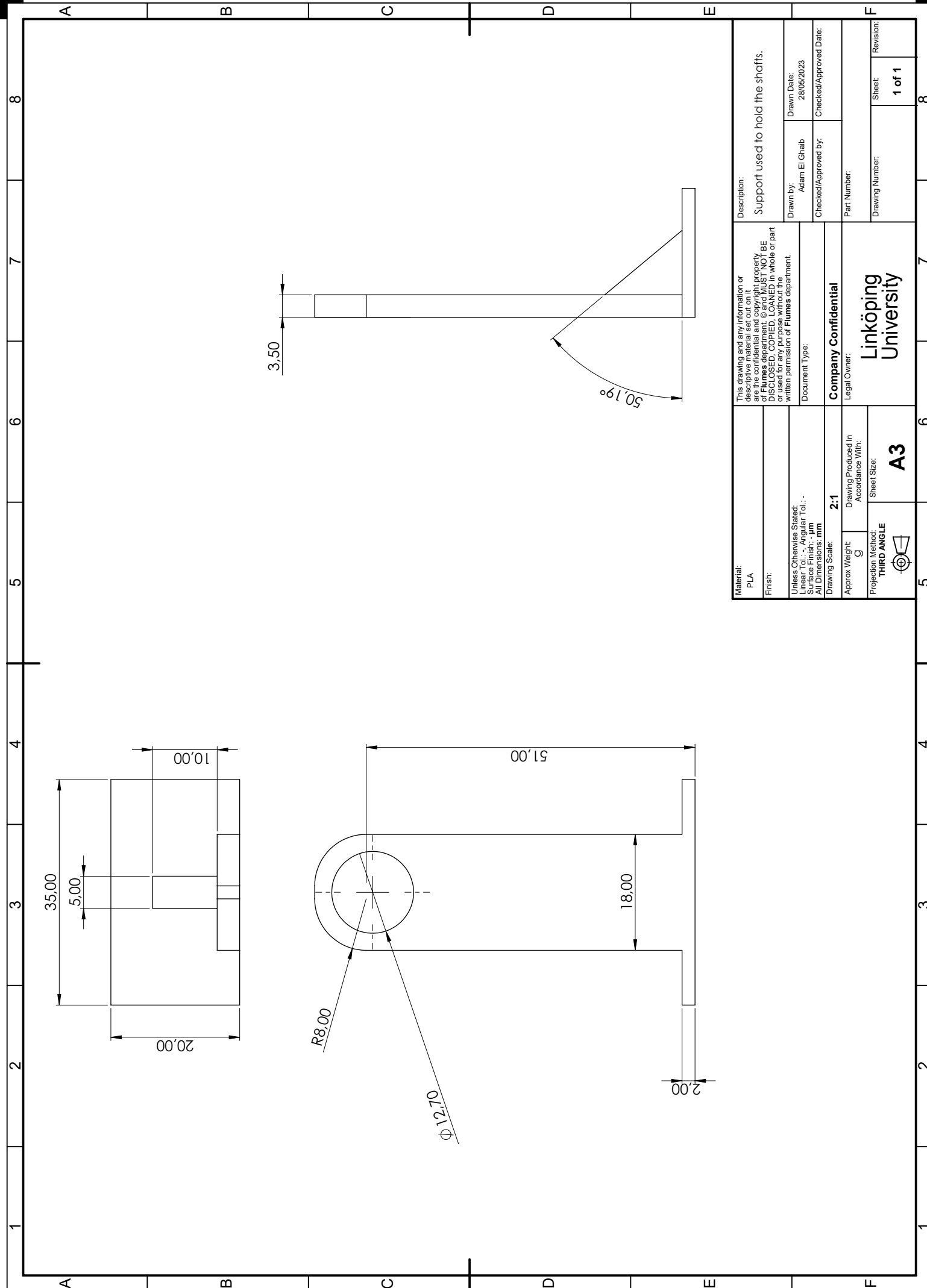

Appendix B

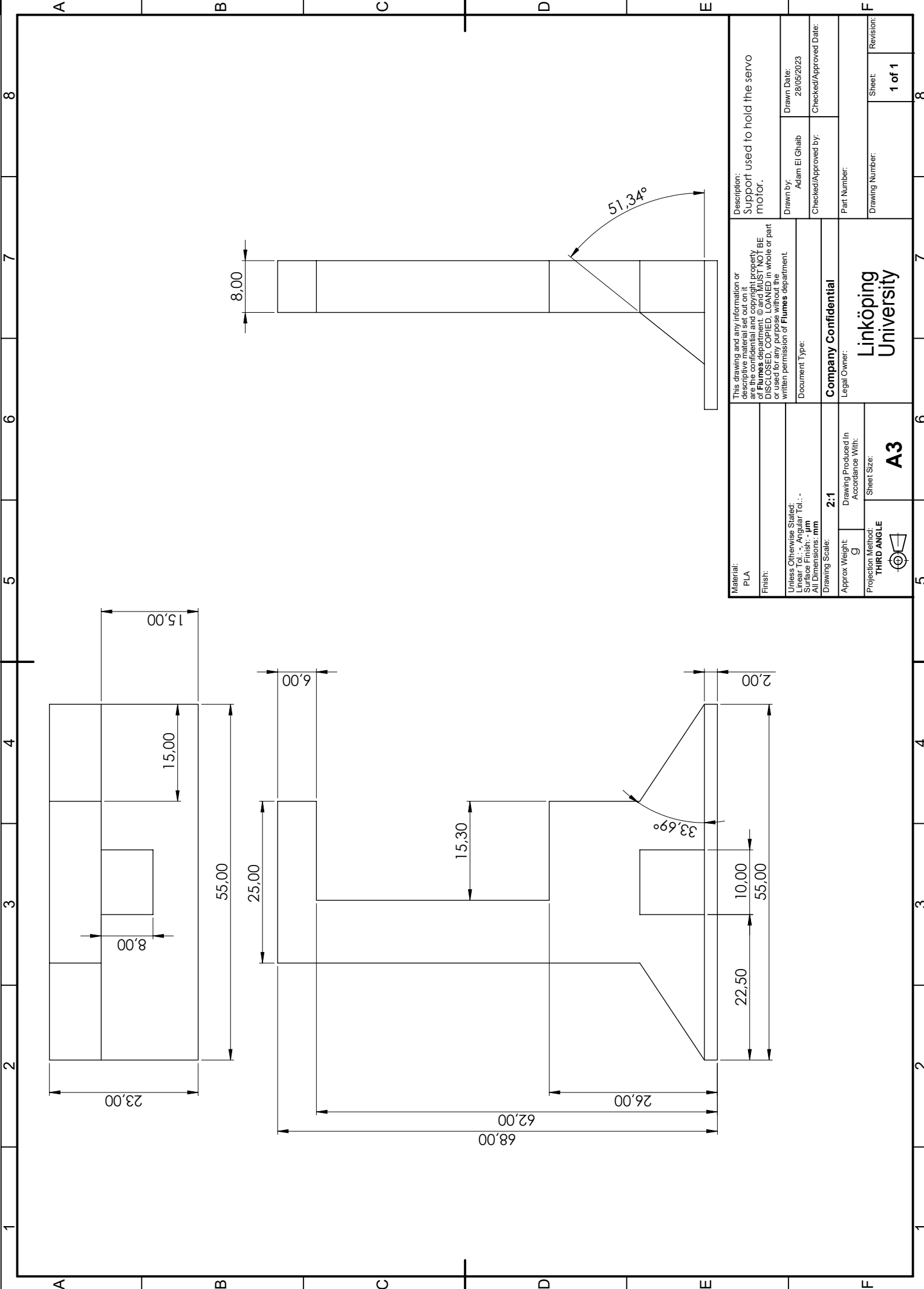
Drawings

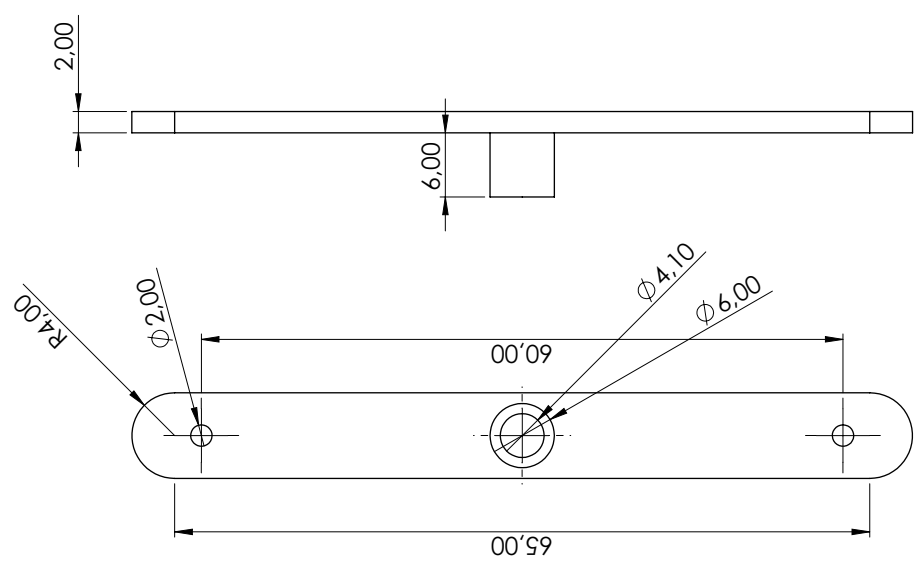


Airfoil: NACA 64-006

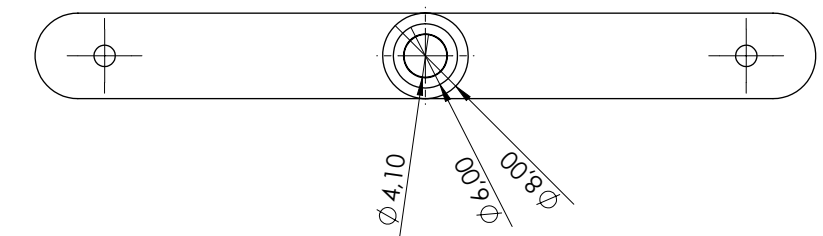
Material:	PLA	Description:	
Finish:		This drawing and any information or descriptive material set out on it are the confidential and copyright property of Flume's department. © and All rights reserved. No part of this drawing may be reproduced without the written permission of Flume's department.	
Unless Otherwise Stated:		Drawn by:	Adam El Ghrib
Linear Tol.: - ; Angular Tol.: -		Checked/Approved by:	28/05/2023
Surface Finish: μm		Drawn Date:	
All Dimensions: mm		Document Type:	
Drawing Scale:	1:1	Company Confidential	
Approx Weight:	Drawing Produced In	Legal Owner:	
200 g	Accordingance With:	Linköping University	
Projection Method:		Sheet Number:	1 of 1
THIRD ANGLE	Sheet Size:	Revision:	
	A3		



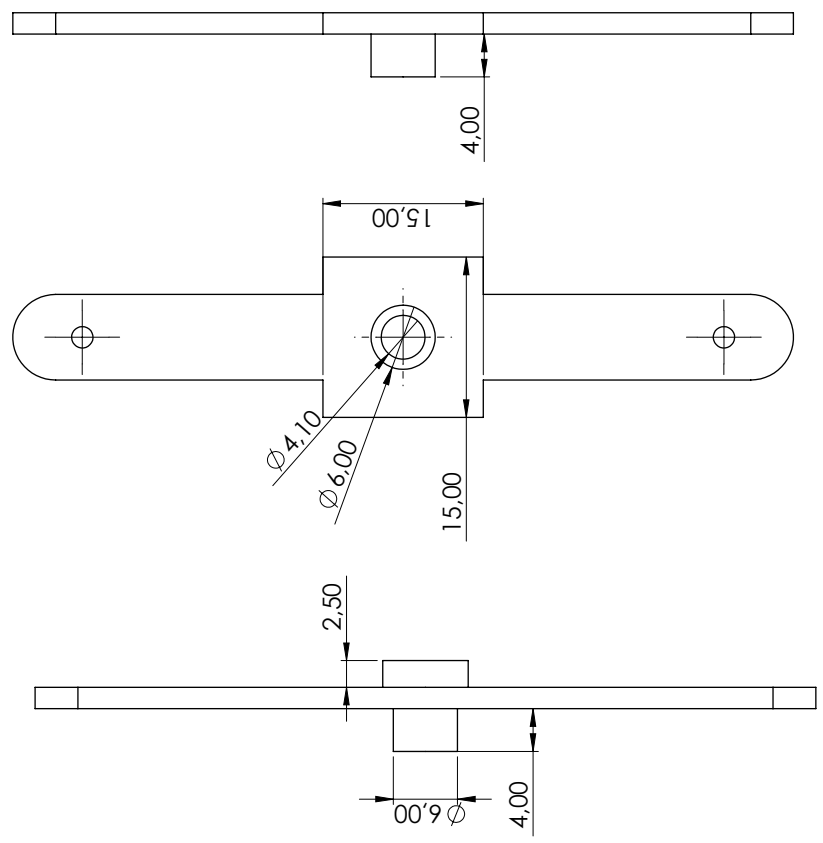




Right Lever

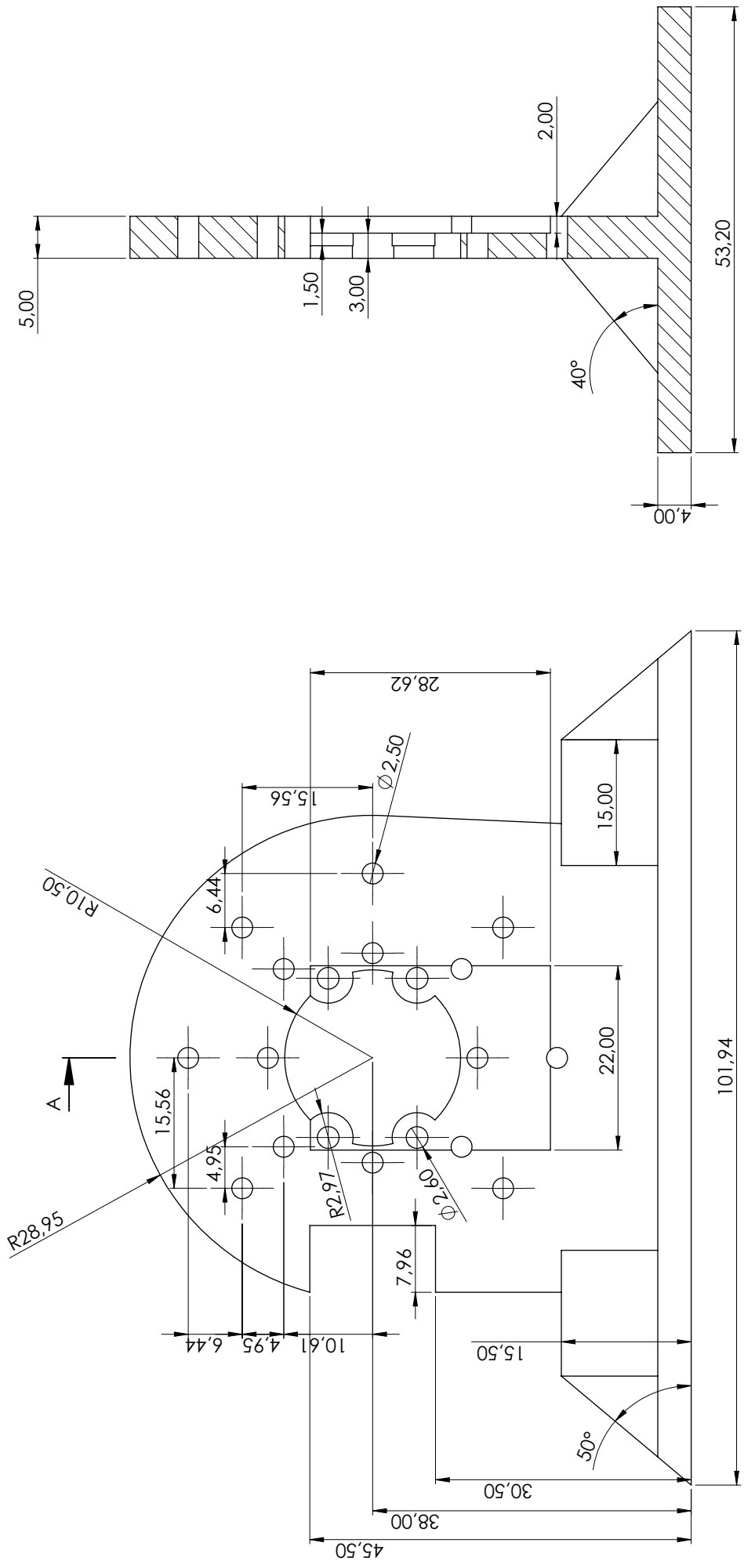


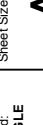
Inner left lever



Outer left lever

Material:	PLA	Description:	Levers used to transmit torque and to hold the magnetic sensor.
Finish:		Drawn by:	Adam El Ghrib
Unless Otherwise Stated: Linear Tol.: - ; Angular Tol.: - Surface Finish: μm All Dimensions: mm		Checked/Approved by:	28/05/2023
Drawing Scale:	2:1	Part Number:	
Approx. Weight	Drawing Produced In Accordance With:	Drawing Number:	Revision:
g		A3	1 of 1
Projection Method: THIRD ANGLE	Sheet Size:	Sheet:	



Material: PLA	This drawing and any information or descriptive material set out on it are the confidential and copyright property of Flumes department, © and MUST NOT BE DISCLOSED, COPIED, LOANED in whole or part or used for any purpose without the written permission of Flumes department.			Description: Support to hold the BLDCM and magnetic sensor.
Finish:				Drawn Date: 28/05/2023
Unless Otherwise Stated: Linear Tolerance: - Surface Finish: - μm All Dimensions: mm				Checked/Approved By: Adam El Ghalb
Drawing Scale: 2:1				Part Number: Drawing Number: Linköping University
Approx Weight: g	Drawing Produced In Accordance With:			Sheet 1 1 of 1
Precision Method: THIRD ANGLE	Sheet Size: A3			

Producto SOLIDWORKS® Educational. Solo para uso en la enseñanza.